NASA CR-72810

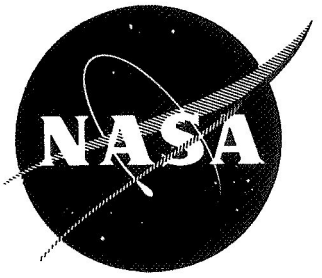

EXPERIMENTAL VERIFICATION OF THE DESIGN OF A HIGH EFFICIENCY LINEAR INJECTED BEAM CROSSED-FIELD AMPLIFIER

by

C.L. Jones and R.W. Herriott

LITTON INDUSTRIES
ELECTRON TUBE DIVISION
SAN CARLOS, CALIFORNIA

Prepared for

NATIONAL AERONAUTICS AND SPACE ADMINISTRATION

NASA LEWIS RESEARCH CENTER
CONTRACT NAS 3-11529
PETER RAMINS, PROJECT MANAGER

NOTICE

This report was prepared as an account of Government sponsored work. Neither the United States, nor the National Aeronautics and Space Administration (NASA), nor any person acting on behalf of NASA:

A) Makes any warranty or representation, expressed or implied, with respect to the accuracy, completeness, or usefulness of the information contained in this report, or that the use of any information, apparatus, method, or process disclosed in this report may not infringe privately owned rights; or

B) Assumes any liabilities with respect to the use of, or for damages resulting from the use of any information, apparatus, method or process disclosed in this report.

As used above, "person acting on behalf of NASA" includes any employee or contractor of NASA, or employees of such contractor, to the extent that such employee or contractor of NASA, or employee of such contractor prepares, disseminates, or provides access to, any information pursuant to his employment or contract with NASA, or his employment with such contractor.

Request for copies of this report should be referred to:

National Aeronatuics and Space Administration
Office of Scientific and Technical Information
Attention: AFSS-A
Washington, D. C. 20546

NASA CR- 72810

FINAL REPORT

EXPERIMENTAL VERIFICATION OF THE DESIGN OF A HIGH EFFICIENCY LINEAR INJECTED BEAM CROSSED-FIELD AMPLIFIER

by

C.L. Jones and R.W. Herriott

LITTON INDUSTRIES
ELECTRON TUBE DIVISION
960 INDUSTRIAL ROAD • SAN CARLOS, CALIFORNIA

Prepared for

NATIONAL AERONAUTICS AND SPACE ADMINISTRATION

August 5, 1970

NASA Lewis Research Center
Cleveland, Ohio
Peter Ramins, Project Manager

TABLE OF CONTENTS

FIGURES

ABSTRACT

This report discusses the design of a long life (greater than 2 years), high efficiency linear injected beam crossed-field amplifier including a ten stage depressed collector. The cw design is experimentally verified in a low duty demountable amplifier. A collector efficiency in excess of 87 percent and a plate efficiency, i.e. overall efficiency, greater than 65 percent at 5 kw peak output power and 2 GHz are demonstrated along with a 10 percent saturated 3 db bandwidth.

Methods other than the depressed collector are evaluated for improving the overall efficiency of the device. These methods include potential limiting, phase focusing and beam prebunching. Potential limiting is shown in the experimental amplifier to be a method leading to significant overall efficiency enhancement if no other collector is used.

SECTION 1

SUMMARY

In this report, a design procedure is discussed for a high efficiency linear injected beam crossed-field amplifier (IBCFA), including a ten stage depressed collector. The collector makes available for recovery on depressed electrodes as much as 90 percent of the spent beam kinetic power, and the ten elements recover as much as 90 percent of the potential power in the spent beam at the end of the collector region. The emphasis in the design procedure is placed on low cathode loading for long life (greater than 2 years), minimum rf and beam dissipation for highest overall efficiency, and the capability of 4 kW cw output power with conduction cooling at 2 GHz with at least 30 MHz 3 db bandwidth and 16 db gain.

A demountable low duty experimental amplifier is described and used for experimental verification of the amplifier and collector designs. The collector design is verified with a measured collector efficiency in excess of 87 percent for a predicted 89 percent. The desired plate efficiency, i.e., overall efficiency, of 65 percent at 2 GHz and 5 kw peak output power is also demonstrated. As expected, the saturated bandwidth is shown to be 200 MHz at 2 GHz. At reduced output power (reduced beam current), a linear rf dynamic range of 40 db up to 3 db below saturation is measured at 2 GHz with a signal to noise ratio rising to 52 db and a maximum second harmonic power which is 34 db down. The collector is demonstrated to operate

methods include potential limiting, phase focusing and beam prebunching. The experimental amplifier is used to demonstrate that potential limiting can significantly enhance the overall efficiency of an IBCFA.

SECTION 2

INTRODUCTION

The work in this report follows work done previously under NASA Contract NAS 3-11513[1]. The previous work examined many different slow-wave circuits which are suitable for use in a linear injected beam crossed-field amplifier (IBCFA). An analytical design was carried out for a 5 kW cw IBCFA operating at 2 GHz with a 30 MHz bandwidth, high interaction efficiency and suitable for long life (greater than 2 years) space borne communications applications. In addition, a ten stage depressed collector was designed to achieve maximum plate efficiency from the device. The previous work also qualitatively examined methods other than the depressed collector for increasing the efficiency of the IBCFA. These methods included potential limiting, phase focusing and beam prebunching.

The current effort is carried-out to experimentally verify the design concepts advanced in the previous work. The objective is to demonstrate 5 kw peak output power at 2 GHz with at least 30 MHz 3 db saturated bandwidth and 65 percent plate efficiency, i.e. overall efficiency, in a low duty demountable amplifier, and to demonstrate efficiency enhancement by phase focusing, potential limiting and beam prebunching. The basic amplifier design should be capable of operating cw with conduction cooling.

This work represents a significant departure from past IBCFA development and demonstrates the application of the IBCFA to space

communications. The bandwidth is reduced from the 40 percent to an octave or more, typical of IBCFA's used in radar and ECM applications, and the efficiency is no longer just moderately high. The size and weight are reduced for the power level and frequency of operation and the life is extended.

The design procedures presented in this report and the efficiency enhancement techniques (potential limiting in particular) should prove useful in all IBCFA designs. Potential limiting not only should improve the efficiency of an IBCFA, but also should produce a more linear gain characteristic for AM applications. In addition, the collector described in this report should be a valuable tool for analysis of crossed-field beams.

SECTION 3

DEVICE DESCRIPTION

The crossed-field interaction between a growing rf wave on a slow-wave circuit and electrons moving in synchronism with it is basically a potential power exchange. Potential power from the moving electrons is given up to the growing rf wave. The average electron velocity or drift velocity, given by the ratio of dc electric to perpendicular dc magnetic field, E_o/B_o, remains nearly constant throughout the interaction in a direction perpendicular to both dc fields.

This type of traveling-wave interaction is inherently quite efficient. Since the electron velocity does not change significantly, synchronism between the growing wave and the drifting electrons can be maintained throughout the interaction, and nearly all of the power in the moving electrons can be extracted.

The amount of power which can theoretically be extracted from the drifting electrons in this type of interaction is that portion of the total power which is potential. Assuming univelocity electrons, this portion is given by the electronic efficiency $\eta_e=1-V_o/E_{b2}$ where V_o is the voltage through which the beam is accelerated from the cathode and E_{b2} is the slow-wave circuit potential relative to the cathode. In this case, that portion of the power which is kinetic, V_o/E_{b2}, is dissipated on the slow-wave circuit when all electrons are collected there. The electronic efficiency in a crossed-field interaction can in practice be made quite high (greater than 90 percent).

The specific type of crossed-field interaction with which this report deals is of the forward-wave non-reentrant, injected beam type. The electrons are injected into an interaction region in which the rf wave grows in the direction of the beam motion (forward-wave). As the beam loses potential, it moves toward the slow-wave circuit and is collected. (Figure 1). Any portion of the beam that is not collected on the circuit is collected on some type of collector at the end of the interaction region (non-reentrant).

Figure 1 illustrates the normal voltages and currents in a forward-wave, non-reentrant IBCFA. Normally there is no accelerator current, i_{b1}, grid current, i_g, or sole current, i_{so}. The beam current, i_b, is the sum of all the other currents in the system. The sole voltage, E_{so}, and the grid voltage, E_g, are usually negative with respect to cathode. It is important to note that, in the calculation of efficiency, collection of electrons on elements more negative than the cathode (sole, grid and some collector elements) is assumed to be useful power. Power supplies for these elements must transform electrical power to different potentials. These complicated power supplies become practical in spaceborne applications when the added system efficiency outweighs the increased complication.

$$\eta_p = P_0/\left(P_{in} + E_{b2}\, i_{b2} + \sum_{n=1}^{N} E_{cn}\, i_{cn} + E_f\, I_f + E_{so}\, i_{so} + E_{b1}\, i_{b1} + E_g\, i_g\right)$$

$$i_b = i_{b2} + \sum_{n=1}^{N} i_{cn} + i_{so} + i_{b1} + i_g$$

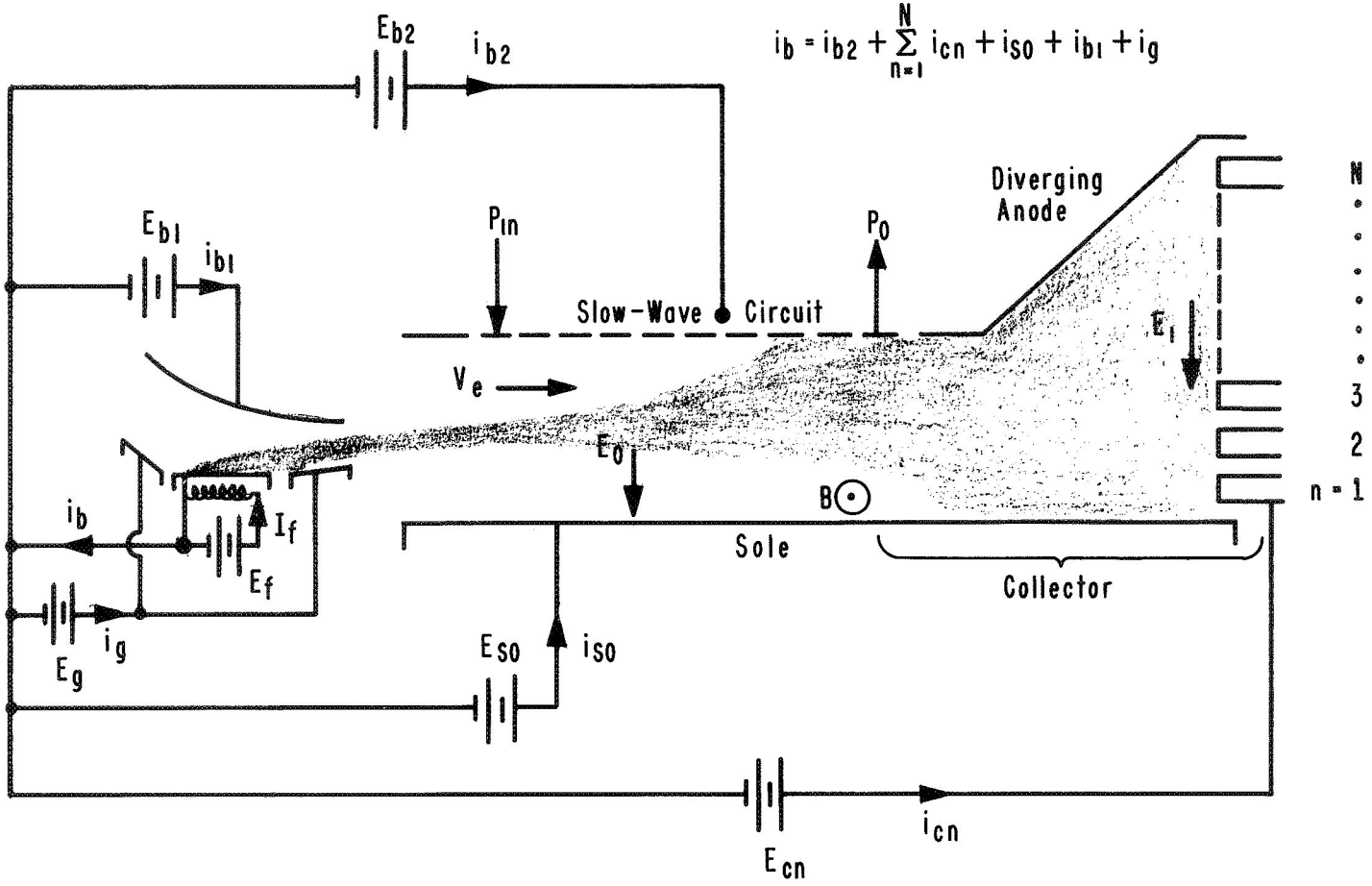

Forward-Wave Non-Reentrant IBCFA Schematic A142

Fig. 1

SECTION 4

OPTIMIZATION STUDIES

This device is represented as converting an input dc and rf power to a useful dc as well as rf output power. The dc input power is thus reduced by the amount of useful dc output power produced. It follows that the plate efficiency (overall efficiency), η_p, of the device can be written in terms of the losses which take place in the device.

The losses in this device are of two kinds. First is the dissipation of beam kinetic power upon collection by an element in the device. The second is the rf attenuation of the slow-wave circuit, α_T. The losses due to beam dissipation on the circuit depend on the electronic efficiency, η_e, and in the collector on collector efficiency, η_{col}. The plate efficiency, i.e., overall efficiency, of the amplifier can now be written in a useful form in terms of the losses, assuming $i_g = i_{so} = i_{b1} = 0$.

$$\eta_p = 1/\left[1 + \frac{i_{b2}}{i_b}\left(1 - \frac{\eta_e}{K}\frac{E_{b2}i_b}{p_o} + \frac{\alpha_T}{p_o} + \frac{p_{col}}{p_o}(1-\eta_{col})\right)\right] \qquad (4\text{-}1)$$

All losses are relative to the output power, p_o. K is the electronic efficiency degradation factor (greater than 1) and p_{col} is the beam power input into the collector region. Equation (4-1) indicates all of the losses in the device which affect plate efficiency (overall efficiency). The first term in the denominator is the beam dissipation losses on the circuit. The second term is the rf losses on the circuit and the third term is the beam dissipation losses in the collector.

In the optimization studies all of the losses are balanced to give the best possible overall efficiency. The best slow-wave circuit and collector designs are found and the amplifier design is selected to achieve the proper balance among all of the various loss mechanisms. Of course, a better circuit or collector design would give a higher overall efficiency. Short of adding more electrodes, which might become mechanically unfeasible, the collector design in this report is believed to be the best possible while maintaining rf dynamic range. Both the basic collector design and various slow-wave circuits were extensively examined on the previous contract and those adopted found to be optimum.

It may be of interest to summarize the final balance of the various losses in the device in the optimum design. For an rf output power of 5 kw and a total input power of 6.90 kw, the rf dissipation on the circuit is 0.51 kw, the beam dissipation on the circuit is 0.94 kw, the beam dissipation on the collector is 0.32 kw, and the power lost due to the filament is 0.03 kw. The optimum design is approaching the ideal case where the only loss is beam dissipation on the circuit. In this case the plate efficiency (overall efficiency) is equal to the electronic efficiency.

Equation (4-1) reduces to $\eta_p = \eta_e$ under certain conditions. These conditions consist of no slow-wave circuit attenuation, no electronic efficiency degradation, complete collection on the circuit (anode current equals beam current), and infinite gain.

There is one very basic difficulty in achieving the conditions for $\eta_p = \eta_e$. While the infinite gain requirement can be closely approached with gains of 20 db or more, the presence of significant slow-wave circuit attenuation makes all other conditions impossible to approach. The degradation of electronic efficiency increases at higher gain rates because the beam is accelerated more rapidly toward the circuit giving it a significant added velocity in that direction. To overcome this added velocity, the line becomes long and the rf losses high with finite circuit attenuation. Also, it is well known that to achieve complete circuit collection the line becomes even longer and the losses higher.

Since complete circuit collection is impractical due to circuit attenuation, it becomes desirable to add a collector to recover as much of the spent beam as possible. Referring to equation (4-1), the approach in these optimization studies is first to optimize the slow-wave circuit and the basic crossed-field interaction for minimum α_T/p_o consistent with other design considerations. The minimum α_T/p_o is found to be only a function of η_e and decreases with decreasing η_e. Next, the collector is optimized for maximum η_{col} consistent with other design considerations. And last, large signal computer calculations are made to determine the optimum η_e and degree of saturation ($E_{b2}i_{b2}/p_o$) for the collector efficiency obtained to give the highest η_p.

4.1 Interaction Circuit

The characteristics of an interaction circuit only become important

when considered with respect to the basic interaction equations under which it will be used and the requirements of the amplifier design to be obtained. The essential requirements of the amplifier are 16 db gain, a cw output power capability of 5 kW, a 3 db bandwidth (B.W.) of 30 MHz at 2 GHz (1.5 percent), a cathode loading of less than one ampere per square centimeter for greater than 2 years life, and maximum plate efficiency (overall efficiency). Assuming synchronism, beam injection at or near the center of the interaction space between sole and line, and low attenuation compared to the gain, there is one basic interaction equation:

$$\text{Gain (db)} = 20 \log \left[\frac{\cosh 2\pi D N \sqrt{1+s^2} + S^2}{1 + S^2} \right] \tag{4-2}$$

$$D = \left[\frac{2\pi f_o i_b K_o \sinh 2\beta x_o}{4\eta V_o B_o \sinh^2 \beta a} \right]^{1/2} \tag{4-3}$$

$$S = \frac{i_b}{4\varepsilon_o B_o \eta H V_o D} \tag{4-4}$$

The gain depends on the gain parameter D and the space charge parameter S. These parameters in turn are dependent on the beam current i_b, the dc magnetic field B_o, the electron charge to mass ratio η, the frequency f_o, the circuit propagation constant β, the beam voltage V_o, the beam width in the direction of magnetic field H, the distance the beam is injected from the sole x_o, the sole to circuit gap a, and the circuit interaction impedance K_o.

If the line length in wavelengths, N, is fixed, the gain given by equation (4-2) assumes the beam position x_o, and the beam current i_b, are constant. This is only true if the gain is small signal, i.e., the rf power on the line is small compared to the beam power (low efficiency). Large signal gain is usually found by solving the force equations incrementally on a high speed digital computer. However, a useful empirical formula which has been found to agree very closely with computer calculations of large signal gain is given by equation (4-2) with the space charge parameter $S = 0$.

For a given saturated gain the product DN is fixed. The value of S then gives the small signal gain for that design. The maximum value of S is determined by stability considerations. With an input and output VSWR of 1.05:1, S may be as high as 3 for 16 db saturated gain design, assuming a comparable load mismatch. However, a value of S as high as 3 means that the linear gain region of the device would occur far below the saturated output power and at low efficiency. A more realistic limiting value of S is 1.5 for applications where linear rf dynamic range is desired at 16 db saturated gain, or in this demountable apparatus where a 1.05:1 VSWR is very difficult to achieve. Operating at values of S higher than indicated eliminates the possibility of wide rf dynamic range since the amplifier will generally be unstable below the drive power required for saturation.

For higher values of saturated gain, the maximum value of S which can be used to maintain linear rf dynamic range to a given level below

saturation decreases. It will be shown in the discussion to follow that the rf losses in the device are directly proportional to S. Therefore, reduced values of S lead to lower plate efficiency (overall efficiency) and, consequently, higher saturated gain leads to lower overall efficiency. A 10 db increase in saturated gain may lead to as much as a 10 percentage point decrease in overall efficiency and, likewise, a 10 db decrease in saturated gain may lead to as much as a 10 percentage point increase in overall efficiency.

Equations (4-3) and (4-4) may be combined in a useful form.

$$S = D/\left(H\epsilon_o 2\pi f_o K_o \frac{\sinh 2\beta x_o}{\sinh^2 \beta a}\right) \tag{4-5}$$

If equation (4-5) is multiplied by αN, where α is the circuit attenuation in db per wavelength, and divided by S, then the result is proportional to the total rf losses, $\frac{\alpha_T}{p_o}$ in db, for constant saturated gain ($\sim$ DN) assuming the hot circuit losses are proportional to the cold circuit losses.

$$1 + \frac{\alpha_T}{p_o} \sim \frac{\alpha_T}{p_o} \sim \alpha N = \alpha\sqrt{V_o}\, DN/\left(\sqrt{V_o}\, SH\epsilon_o 2\pi f_o K_o \frac{\sinh 2\beta x_o}{\sinh^2 \beta a}\right) \tag{4-6}$$

The square root of the beam voltage, V_o, was included in this expression because the product $\alpha\sqrt{V_o}$ is constant regardless of V_o, as will be shown subsequently.

In optimizing the interaction circuit, we seek to minimize α_T/p_o. For fixed f_o, B_o, and η_e, the last term in the denominator of

equation (4-6) can be maximized with respect to the relative beam injection position, x_o/a. It can be shown (Appendix A) that the maximum value of this term occurs at $x_o/a = .5$, and is a function of B_o, f_o, and η_e.

$$\left[\frac{\sinh 2\beta x_o}{\sinh^2 \beta a}\right]_{max} = 1/\sinh\left[\frac{2\pi f_o}{\eta B_o}\left(\frac{\eta_e}{1-\eta_e}\right)\right] \qquad (4-7)$$

Due to beam motion toward the circuit under large signal conditions the relative beam position varies during the interaction. x_o/a increases from its initial value to unity. For the above reason the best value of x_o/a is slightly less than .5 so that the average relative beam position under large signal conditions is $x_o/a = .5$. The optimum x_o/a is usually about .45. Figure 2 shows a typical computer calculation of plate efficiency for various values of x_o/a. The data in Figure 2 represents one of a set of four different designs which were run with this parameter as a variable, and all designs demonstrated an optimum value of $x_o/a = .45$.

It is clear from equation (4-7) that the higher values of this term are obtained for higher B_o and lower η_e and f_o. Frequency is naturally fixed. The reduction of electronic efficiency to reduce rf loss will be balanced later against the increased beam dissipation which it will cause. The maximum value of B_o will be discussed later.

Returning to equation (4-6), one sees that for minimum rf loss it is desirable to have maximum S, H, V_o and f_o. Frequency is already fixed.

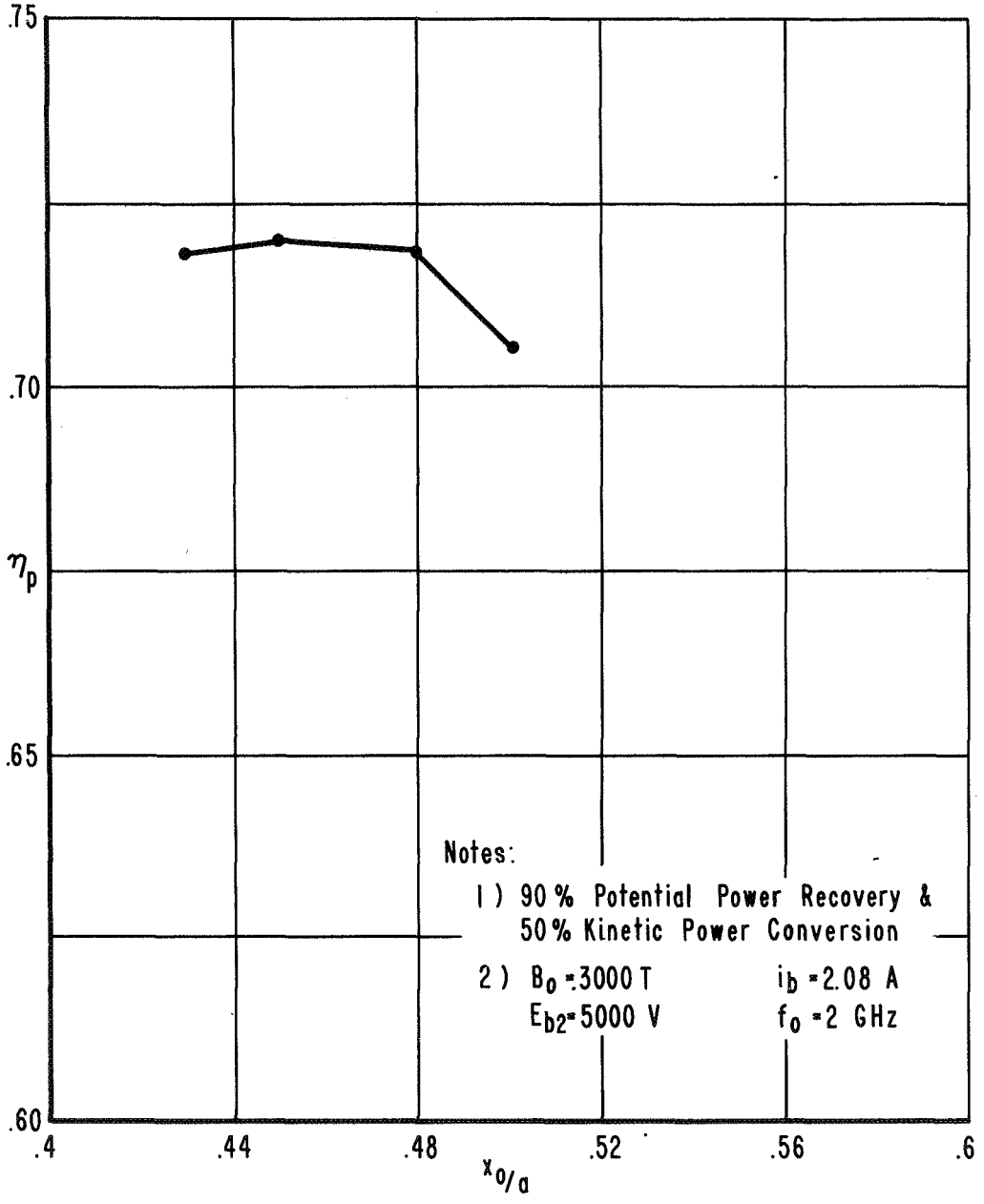

Typical Plate Efficiency VS. Relative Beam Injection Position. D243

Fig. 2

The maximum value of S has been fixed at 1.5 by previous consideration. The maximum value of H is given by the circuit which is used. The maximum value of V_o will be discussed later.

A circuit consideration, in addition to maximum H, which must be made is the minimum of the ratio $\propto\sqrt{V_o}/K_o$. The above circuit considerations suggest a figure of merit $K_oH/(\propto\sqrt{V_o})$ for a slow-wave circuit, and that a good parameter for optimizing a given circuit is $\propto\sqrt{V_o}/K_o$. The Karp[2] circuit has the highest figure of merit of all slow-wave circuits examined. The Karp circuit is a ridge loaded waveguide periodically slotted on the broad wall adjacent to the loading ridge. The Karp circuit is approximately one-half wavelength wide.

Several circuits were built with various loading ridge widths relative to the slot length and various thicknesses of the slotted wall relative to the pitch. The gap to pitch ratio was held constant at 0.5. It was found that the optimum configuration for impedance and bandwidth was a loading ridge width of half the slot length and a small slotted wall thickness (<0.5 pitch). The optimum loading ridge width was predicted by J. C. Walling[4].

The interaction impedance, K_o, and the dispersion characteristics of the circuits (ratio of group to phase velocity, v_p/v_g) were measured by resonance methods[1]. The dispersion results were used with an equation derived by J. R. Pierce[3] to determine $\propto$ for the optimum structure configuration.

$$\alpha = \frac{27.3}{Q} \frac{v_p}{v_g} \qquad (4\text{-}8)$$

The Q of the circuit was calculated from an expression for the stored energy of a Karp circuit by J. C. Walling[4], and the dissipated energy calculated from the fields on a Karp circuit derived by R. C. Fletcher.[5] The attenuation values calculated as described above agree with measurements within 5 percent (Figure 3). The dispersion and impedance for one optimum structure can be scaled easily in frequency and velocity while attenuation can not. The calculation of attenuation makes the optimization of the ratio $\alpha\sqrt{V_o}/K_o$ at 2 GHz possible without construction of many different slow-wave circuits.

Figure 4 shows the calculated variation of $\alpha\sqrt{V_o}/K_o$ with K_o and the phase shift per cell, $\beta p/\pi$, for the optimum Karp circuit at 2 GHz. In the calculation, this ratio was found to be constant regardless of V_o. K_o is independent of V_o, so that the product $\alpha\sqrt{V_o}$ is constant regardless of V_o. This V_o dependence was predicted by J. R. Pierce[3] for an infinitely thin Karp circuit. It is seen in Figure 4 that the ratio $\alpha\sqrt{V_o}/K_o$ decreases for constant $\beta p/\pi$ and increasing K_o. This result is expected since the increase in K_o for constant v_p results from a decrease in group velocity, and K_o increases as the square of $1/v_g$ while α increases as $1/v_g$. It is important to note that this decreasing group velocity for constant phase velocity, $\sqrt{2\eta V_o}$, represents a decreasing bandwidth in the dispersion characteristics of the structure. There is a basic tradeoff between rf losses and bandwidth, and hence efficiency and bandwidth.

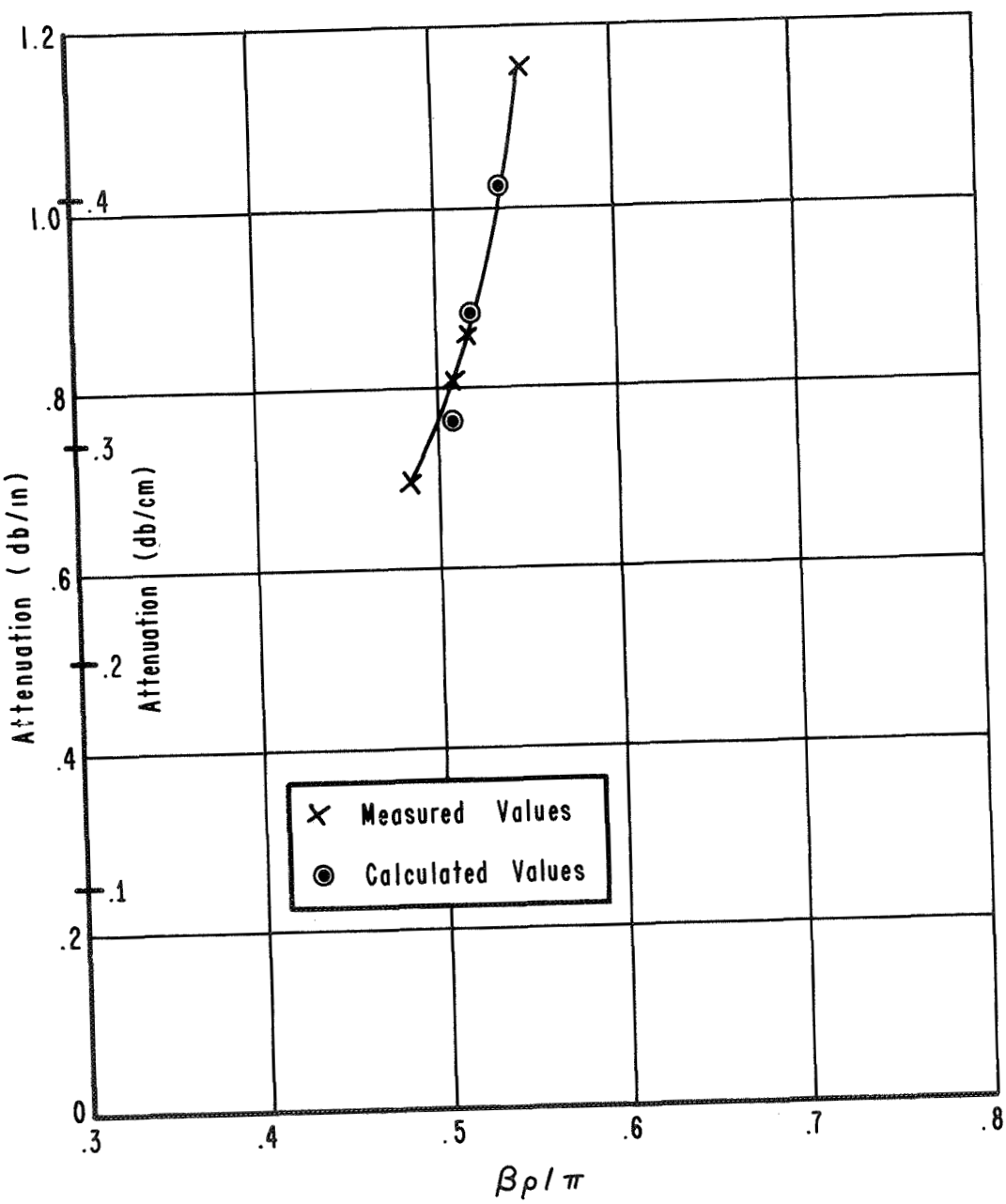

Exp. No. 2A025110 Attenuation D240

Fig. 3

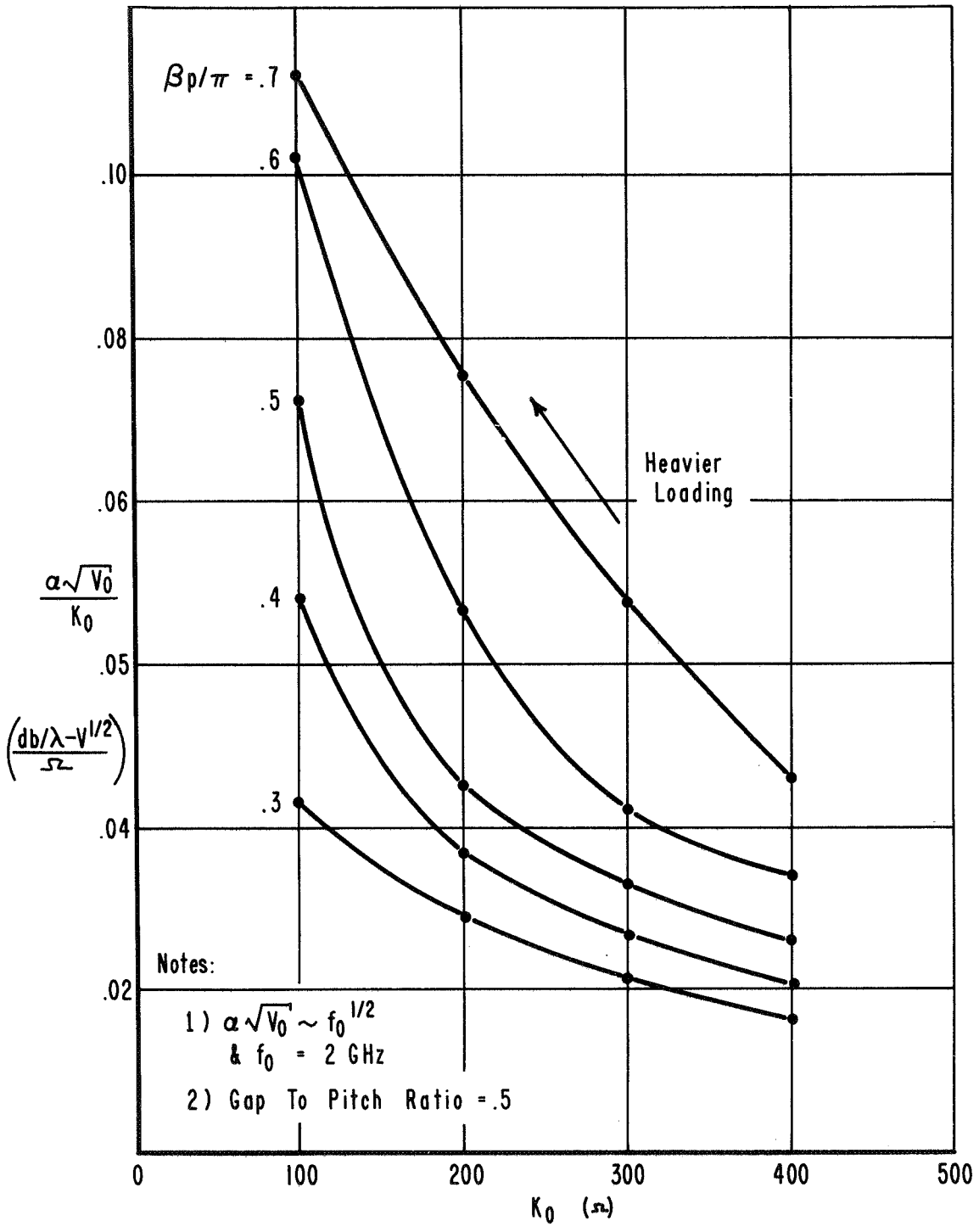

Attenuation For Optimum Karp Circuit D239

Fig. 4

However, bandwidth is not a limiting factor in this design optimization. All circuits have quite ample bandwidth.

The variation of K_o for constant $\beta p/\pi$ in Figure 4 is achieved by variation of the dimension between the loading ridge and the slotted wall. The gap to pitch ratio was held constant for the curves of Figure 4. It is believed that the deviation of $\propto\sqrt{V_o}/K_o$ with $\beta p/\pi$ for constant K_o can be reduced or eliminated by optimizing the gap to pitch ratio for each value of $\beta p/\pi$. This conclusion is in need of more study. The curves of Figure 4 are proportional to the square root of f_o due to decreasing skin depth at higher frequencies.

It appears from Figure 4 that the best operating point is the low value of $\beta p/\pi$ and high K_o. However, thermal considerations must be made. To be consistent with the power level, conduction cooling requirement and present technology, it is necessary to include ceramics under the bars to conduct the dissipated power from the slow-wave circuit. Calculations indicate that the broad Karp circuit can easily handle the power dissipation required through BeO ceramics. These ceramics have two effects. They limit the degree to which the circuit may be unloaded and secondly they reduce the circuit width. It is estimated that the ceramic loading of the circuit will limit the minimum $\propto\sqrt{V_o}/K_o$ to .04 for all $\beta p/\pi$. The minimum $\propto\sqrt{V_o}/K_o$ is the same for all $\beta p/\pi$ with higher K_o and $\propto$ for higher $\beta p/\pi$. The choice of K_o at this point is arbitrary and must be decided as it affects beam dissipation.

It is estimated that the reduction of circuit width will be 30 to 40 percent. Using the half of the circuit which is ridge loaded and reducing that by 40 percent, we find that the maximum width of a 2 GHz Karp circuit is about .900 inch (2.28 cm).

It was shown earlier that for minimum α_T/p_o we desire maximum V_o and B_o. To allow both of these parameters to go to their maximum value it is necessary to allow the dc electric field to be maximum. The maximum electric field E_{max} is given by voltage standoff limits, i.e., the field strength at which arcing becomes a problem. This maximum electric field establishes a relationship between B_o and V_o. $B_o = E_{max}/\sqrt{2\eta V_o}$. Using this relationship, it is possible to find the optimum conditions for B_o and V_o for minimum α_T/p_o in terms of the frequency, which is fixed, and the electronic efficiency η_e (Appendix B).

$$B_o \geq \frac{2\pi f_o(1-\eta_e)}{0.2\eta\,\eta_e} \tag{4-9}$$

$$\sqrt{2\eta V_o} \leq \frac{0.2\eta E_{max}\eta_e}{2\pi f_o(1-\eta_e)} \tag{4-10}$$

It can be concluded from the above solution that V_o should be raised to the maximum value as given by E_{max} for constant B_o and B_o should be as high as possible. The optimum B_o and V_o are infinite and zero respectively; however, if equations (4-9) and (4-10) are observed, the rf losses will change very little with B_o and V_o.

Referring back to equations (4-6) and (4-7), we see that all parameters have been optimized for minimum rf losses except η_e. As η_e decreases, rf losses decrease, and there is a direct trade-off between rf and beam losses. Table 1 summarizes the results for the optimum parameters necessary for minimum α_T/p_o. The assumptions made are also listed in Table 1.

TABLE 1

Optimum Parameters for Minimum α_T/P_o

Parameter	Optimum Value
f_o	fixed = 2 GHz
S	maximum for stability = 1.5
H	circuit maximum = .900 in. = 2.28 cm
$\alpha\sqrt{V_o}/K_o$	circuit minimum = $0.04\ \frac{db/\lambda(V)^{1/2}}{\Omega}$
x_o/a	.45
B	$\geq \frac{2\pi f_o(1-\eta_e)}{0.2\eta\eta_e}$
$\sqrt{V_o}$	$\leq \frac{0.2\eta E_{max}\eta_e}{2\pi f_o\sqrt{2\eta'(1-\eta_e)}}$
K_o	arbitrary
η_e	that for minimum rf + beam losses

Assumptions:

1) The saturated gain is given by only the product DN.

2) The hot circuit losses are proportional to the cold circuit losses.

3) $x_o/a = .5$ for minimum B_o and maximum V_o.

We now seek to select an electronic efficiency and interaction impedance which minimize the total losses in the interaction. As discussed earlier, higher gain rates increase the electronic efficiency degradation factor K. Hence, we should select the minimum K_o possible consistent with low rf losses (K_o = 100Ω at $\beta p/\pi$ = .3 from Figure 4). This low K_o choice also represents the better thermal design since the dissipation on the circuit is over a longer length for lower gain rates and constant saturated gain. The complete dependence of K on other operating parameters was not taken into account in these optimization studies. In general, K will increase as α_T/p_o decreases. This factor K is of some importance and should be studied further.

The electronic efficiency degradation factor is quite difficult to evaluate. As far as can be determined, the only method for calculating K is by rigorous solution of the equations of motion for electrons in the crossed-field beam under large signal conditions. This solution is done numerically on a high speed digital computer. Simple theories which do not include electron acceleration terms (adiabatic) do not predict K. Our computer calculations including space charge indicate that K may be as high as 1.06 for very high gain rates. A value of K = 1.06 degrades an electronic efficiency of 90 percent to 85 percent. Even an approximate relationship between gain per wavelength and K has not yet been established.

Referring to equation (4-1), we must turn to computer calculations to predict plate efficiency. The computer is needed to predict K as well

as the degree of saturation ($E_{b2}i_{b2}/p_o$) to be used in choosing the best η_e for minimum rf plus beam losses. Since the degree of saturation determines the relative power into the collector region, the collector losses should also be considered before choosing the optimum η_e.

4.2 Ten Stage Depressed Collector

The electron drift velocity is given by E_o/B_o. In the ten stage depressed collector for this amplifier (Figure 1), the electron velocity is reduced by a reduction in dc electric field, E_o, caused by the diverging anode. Thus, a portion of the kinetic power contained in the spent beam is made available for recovery on depressed electrodes. Secondary electrons are suppressed and prevented from backstreaming by the forces exerted on them by the dc magnetic field, B_o.

The kinetic power made available for recovery in this collector is given by $1-(E_1/E_o)^2$ where (E_1/E_o) is the ratio of dc electric field at the collector electrode to the dc electric field in the interaction space. The collector in the experimental amplifier makes available 90.3 percent of the beam kinetic power for recovery.

The potential power recovery of this collector, assuming uniform beam potential distribution between elements and uniform element spacing between sole and anode (both in potential and physically), depends on the collector number, n, and the total number of collectors, N. The portion of the beam potential power which is recovered

is given by $1 - \frac{1}{2(N-n+1)}$. The collector in the experimental amplifier has ten elements.

There are two factors which determine the overall collector efficiency, η_{col}, with which the collector in the experimental amplifier operates. The first is the portion of the spent beam power which is potential. It is found empirically from computer calculations that this portion is given by the electronic efficiency η_e. The second is the distribution of the beam between the sole and the line (potential distribution). It is also found empirically that, for this uniformly spaced 10 element collector and any spent beam from a normal interaction, the potential power recovery is almost constant at 90 percent. Hence, for η_e = 90 percent, the collector efficiency is 89.1 percent and collector efficiency is only a function of electronic efficiency, with higher efficiency for higher η_e.

Increased reduction in the dc electric field in the above case could only result in an increase in collector efficiency from 89.1 to 90 percent which is not significant. An increased number of elements would add significant mechanical and power supply complications for relatively small increases in collector efficiency.

The electrodes in this collector could depart from uniform spacing to achieve somewhat higher efficiency under certain conditions. If the level of saturation is chosen and the electrodes moved to optimize efficiency for that spent beam potential distribution,

the efficiency at all other levels of saturation would be reduced because the spent beam potential distribution of an IBCFA changes with saturation level. Since the efficiency increases are small and dynamic range is desirable, it seems best to maintain uniform collector spacing.

4.3 Plate Efficiency (Overall Efficiency)

With an optimized interaction and collector, plate efficiency must now be evaluated with respect to only one variable, η_e, since η_e determines collector losses and both beam and rf circuit losses. Higher η_e reduces beam circuit and collector losses and increases rf losses while lower η_e reduces rf losses at the expense of beam circuit and collector losses. Some optimum value of η_e is expected.

It is important to note that the optimization of the interaction circuit is much more important than the collector optimization since losses in the interaction effect all terms in equation (4-1) because they reduce the output power.

The variation of plate efficiency with electronic efficiency was evaluated with large signal computer calculations including space charge (Figure 5). The plate efficiency was predicted to be a maximum of 72.9 percent at 90 percent electronic efficiency.

Using the very efficient collector, the optimum level of saturation is about 50 percent. That is, about half of the beam is collected on the circuit and half on the collector. Normally, without an efficient depressed collector, about 80 percent of the beam is collected on the line which leads to an overall efficiency in the low 60 percent range.

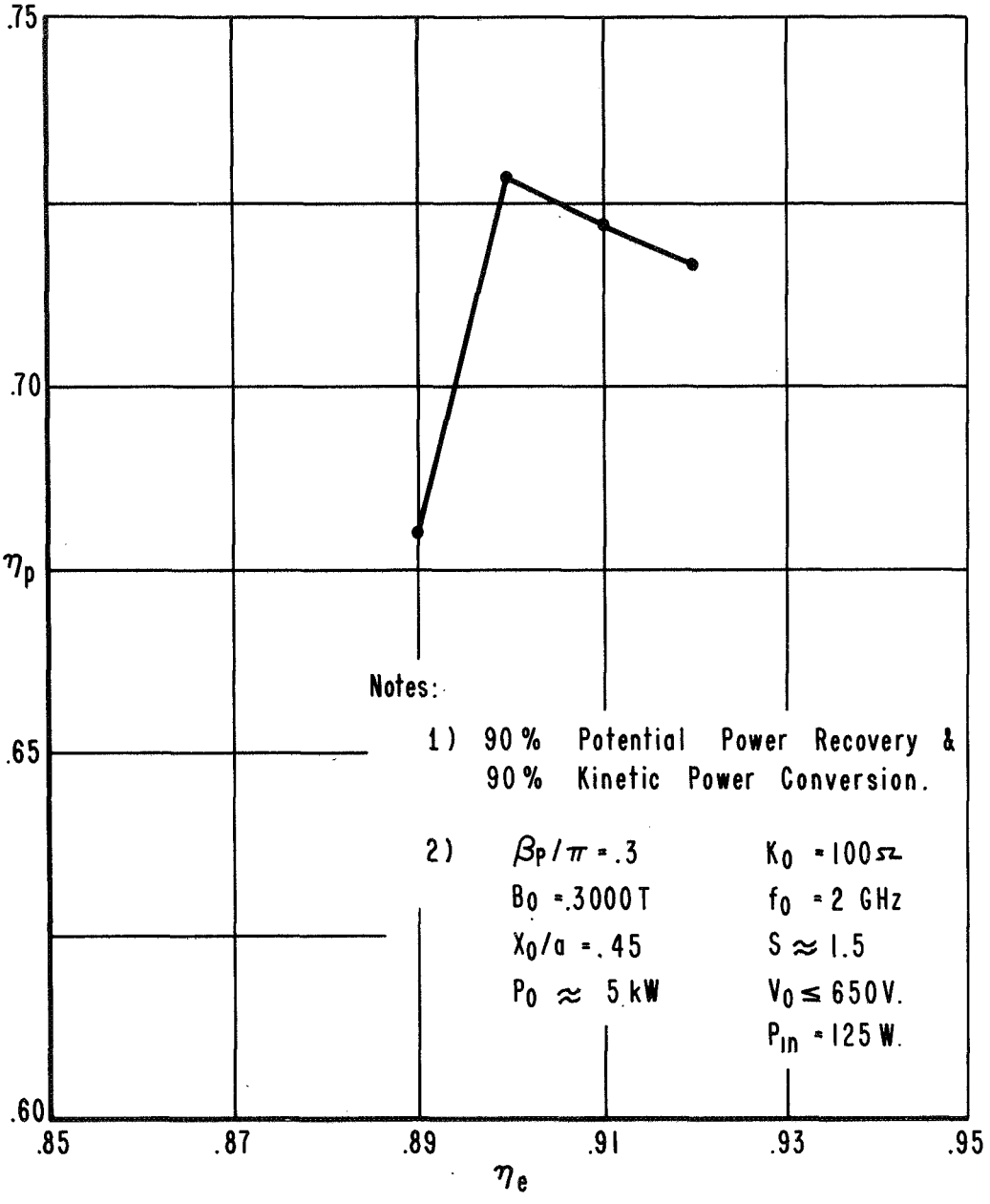

Plate Efficiency VS. Electronic Efficiency D242

Fig. 5

SECTION 5

ASSEMBLY OF THE EXPERIMENTAL AMPLIFIER

The experimental amplifier is made demountable to facilitate changes. Figure 6 illustrates in cross section the experimental amplifier. All parts possible are bolted together. The loading ridge is bolted into the slotted waveguide to form the Karp circuit. The diverging anode is also bolted to the waveguide. The collector elements are stacked and bolted to a support along with the sole insulators. The sole end hats holding a screen sole face are bolted to the insulators. The electron gun (not shown) is bolted to the same support as the sole and depressed collector. The beam is accelerated from the cathode toward the circuit and then turned by the magnetic field to form a ribbon between the sole and circuit.

Figure 7 shows the actual experimental amplifier. The electron gun can be seen in the lower left hand corner looking down on the accelerator blade. The support structure is shown in the background. The circuit is bolted to the back support and the sole support is rotated 90 degrees and bolted to the front support. Coolant flows through the support structure to maintain a minimal amount of cooling. One coolant inlet tube is visible in the upper right hand corner.

A domed cylindrical glass bottle covers the final assembly of Figure 7, and is bolted to the vacuum flange visible in the upper right hand corner. The resulting assembly is bolted to a vacuum chamber and

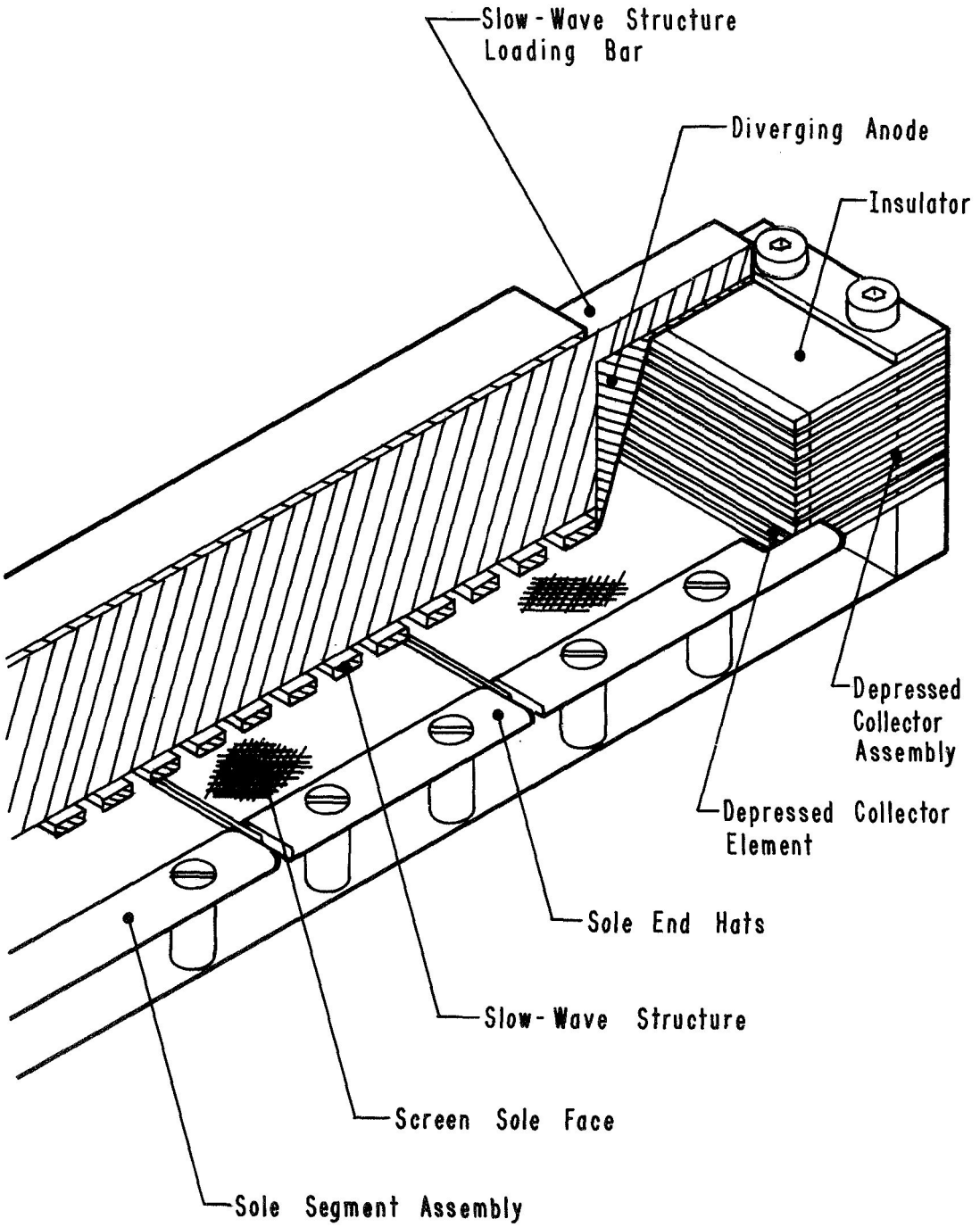
Slow-Wave Structure
Loading Bar
Diverging Anode
Insulator
Depressed
Collector
Assembly
Depressed Collector
Element
Sole End Hats
Slow-Wave Structure
Screen Sole Face
Sole Segment Assembly
Experimental Amplifier
D281

Fig. 6

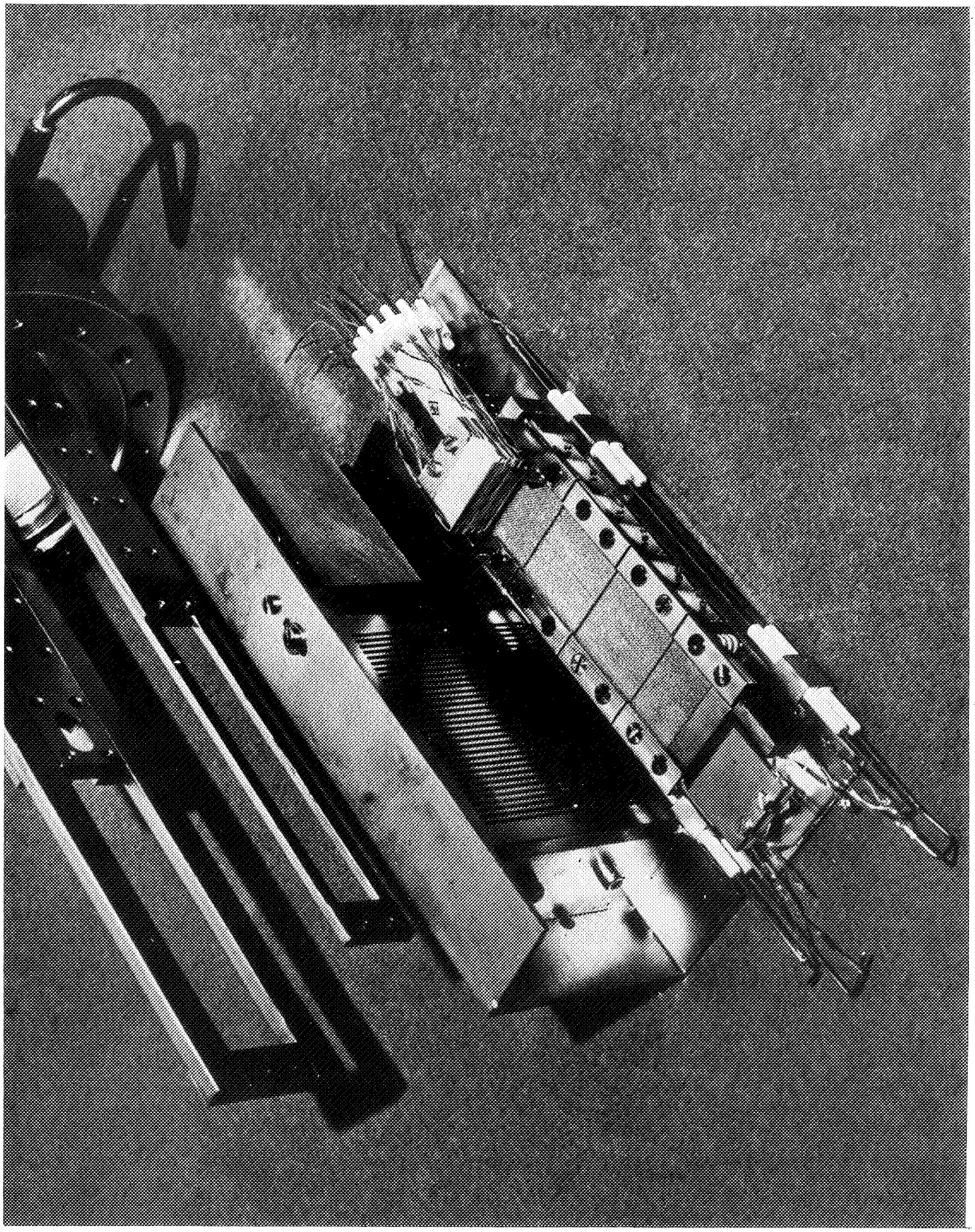

D210

pump. The rf and dc leads exit from the chamber through vacuum seals. The magnetic field is furnished by electromagnets external to the vacuum.

Figure 8 illustrates the electron gun used in the experimental amplifier. The beam is converged to a thin ribbon by the beam forming electrodes on the sides, front and back of the cathode. Figure 9 shows the actual gun. The gun is a modified long Kino[6], low current density design. For ease of assembly, the gun design was taken from an existing IBCFA and is being run at slightly greater than $1A/cm^2$. However, with the beam width available for the Karp circuit, the gun could easily be modified to operate below $1A/cm^2$.

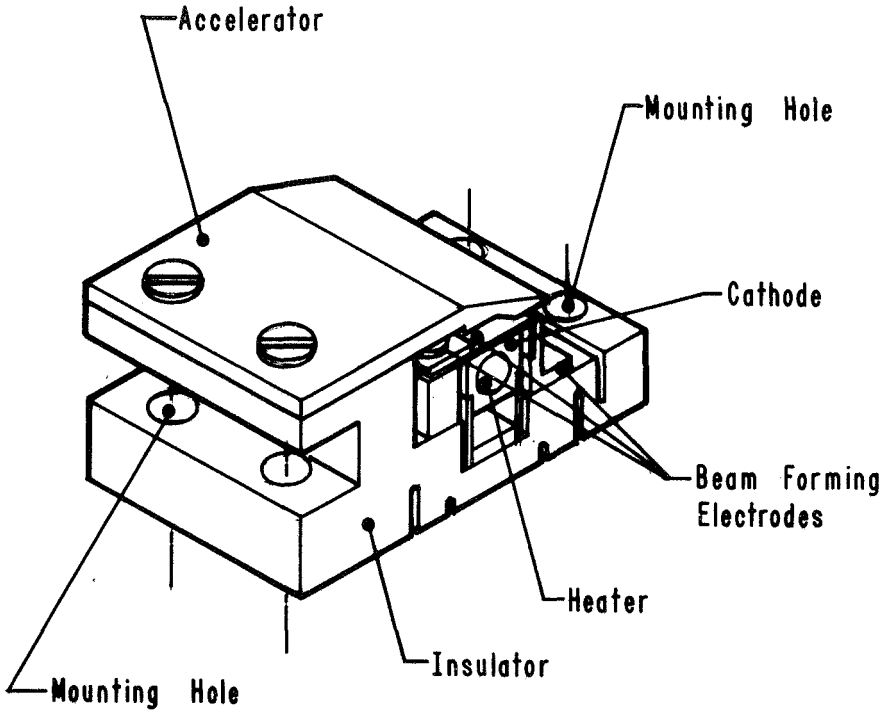

Electron Gun D230

Fig. 8

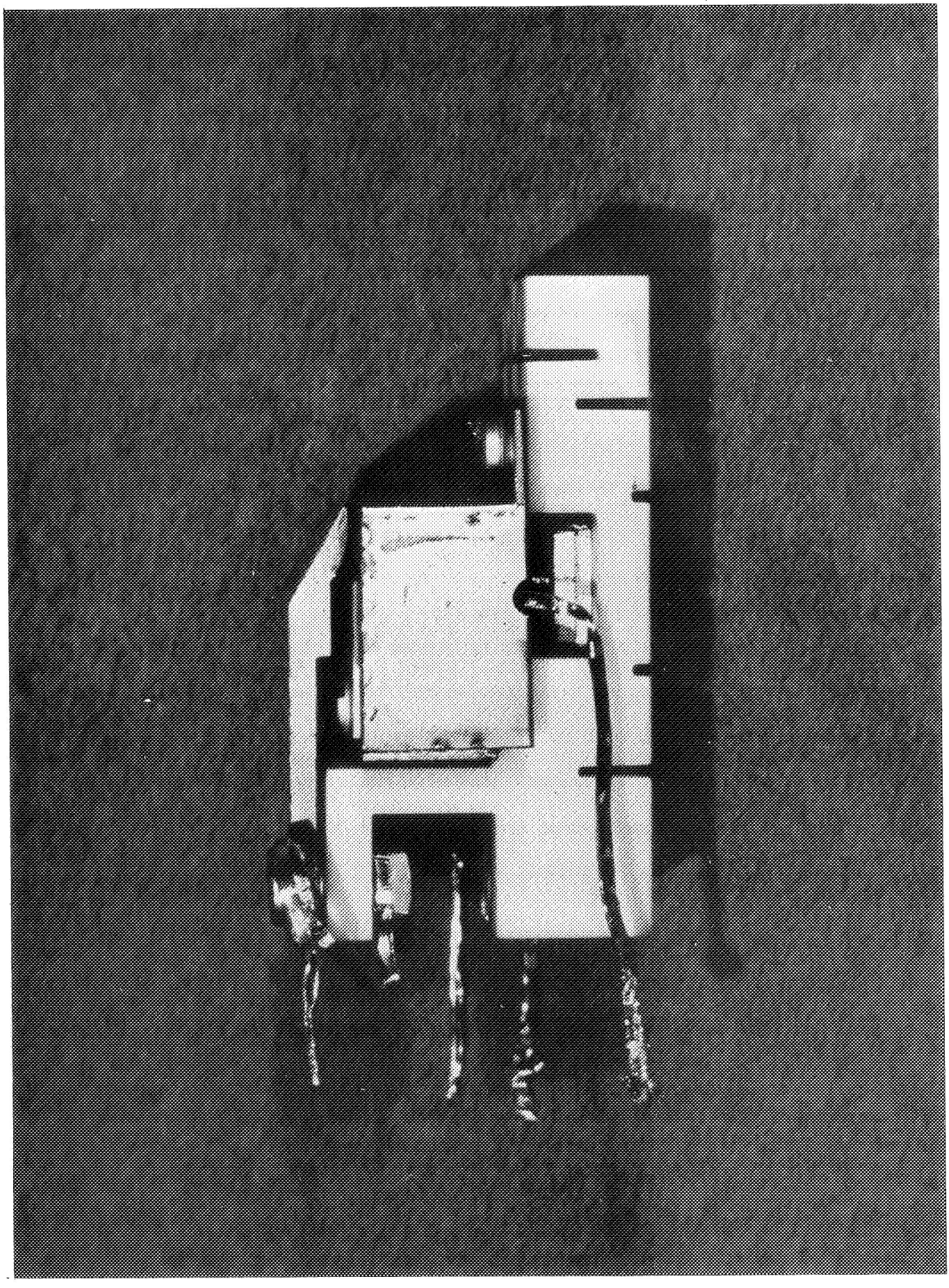

SECTION 6

TEST APPARATUS

Figure 10 illustrates the test set-up used. All rf power and current readings are made with peak reading instruments to increase the measurement accuracy. The peak rf power measurements are traceable to the National Bureau of Standards (NBS) within 5 percent and the peak current and voltage readings within 0.3 percent. Average reading instruments are included for verification only. The low level peak output power measurements are made by means of a signal gain displayed on a spectrum analyzer. The analyzer gain display calibration is traceable to NBS within 0.1 db per 10 db.

The output of all peak detectors is viewed on a time base oscilloscope and nulled against a calibrated millivolt source. The rf crystal detectors were calibrated cw against 60 cycle waterload power at low levels and the power level increased with calibrated attenuators. The pulse current transformer was sent to the manufacturer for a special certified calibration.

Phase measurements were made with a Hewlett Packard Network Analyzer. The input and output sampling arms are eliminated from cold measurements so that non-linearities in the couplers are not included. The phase devation caused by the amplifier beam is then measured and added to the cold measurements. The non-linearities in the rf vacuum seals and related connector are, however, necessarily included.

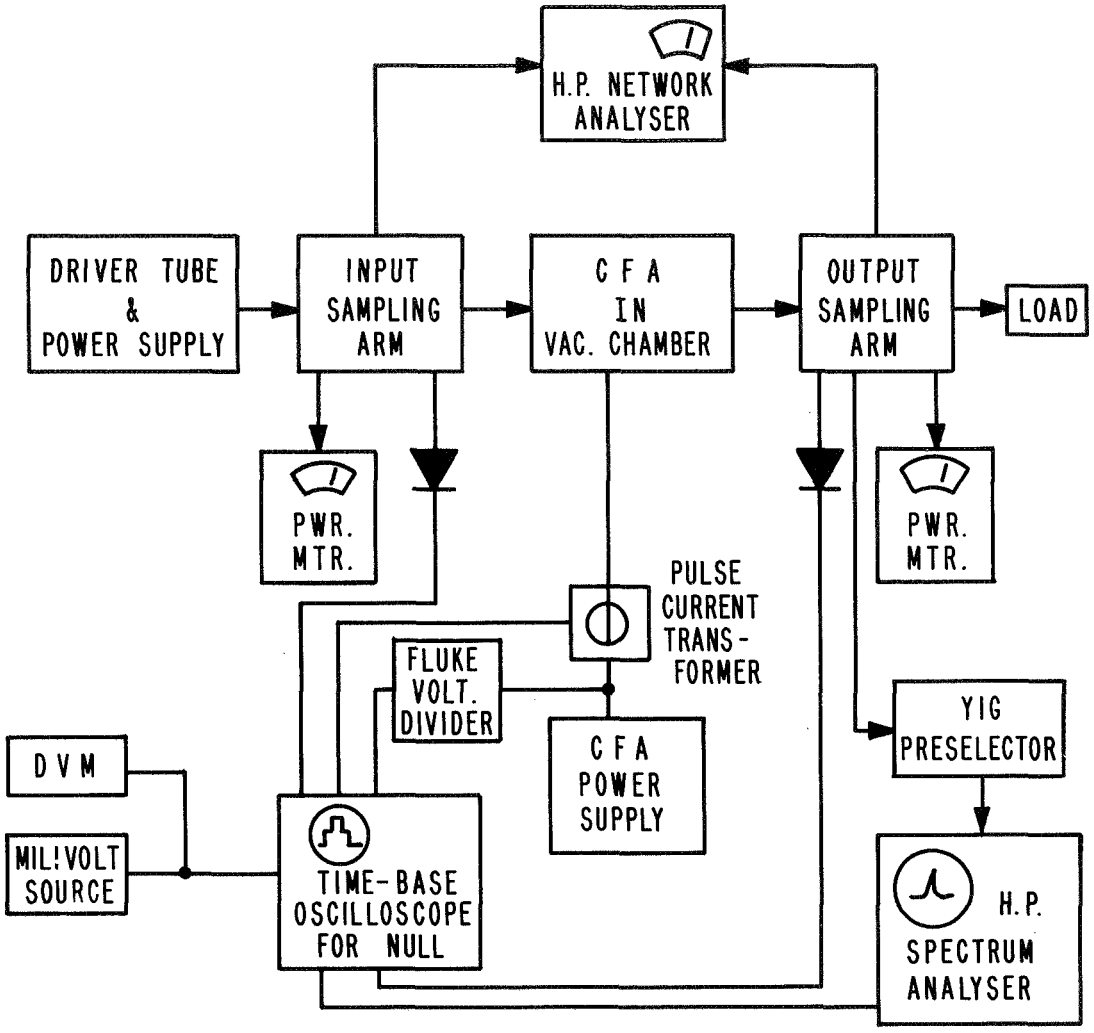

NOTE: ALL R.F. POWER CALIBRATIONS MADE C.W. AGAINST WATER-LOAD POWER AT LOW POWER AND POWER RANGE INCREASED WITH CALIBRATED PADS.

Test Set-Up D231

Fig. 10

SECTION 7

VERIFICATION OF PERFORMANCE

The experimental amplifier was pumped down several times before all mechanical designs and vacuum seals were perfected in the new system. During initial rf testing the collector as well as one of the efficiency enhancement techniques (potential limiting) were experimentally evaluated. The verification of the final amplifier design then followed.

The initial rf tests covered the first 13 pump downs (experiment numbers 2A025101 through 2A025113). The 14th pump down (experiment number 2A016114) evaluated the final amplifier design. The first 9 pump downs had several mechanical problems and vacuum leaks in the new system and no significant data were obtained.

The 10th pump down yielded the first significant data. The bandwidth was verified to be well in excess of the desired 30 MHz on this experiment. An open heater lead terminated this experiment before full output power or plate efficiency (overall efficiency) data were obtained. The heater was changed to a lower current, higher voltage design at this point.

In the 11th pump down, beam viewing was attempted. The vacuum system was brought to a pressure of 3×10^{-5} mm of mercury (4×10^{-3} N/m^2) with helium. However, no evidence of the beam was observed due to

excessive cathode light. This experiment was terminated by severe depressed collector leakage currents before any other data were obtained. A better gas for beam viewing was determined to be krypton, which radiates in the blue and would allow a filter to be used to remove the cathode light.

The 12th pump down was the first experiment to yield plate efficiency (overall efficiency) data. The plate efficiency was found to be substantially less than predicted. The measured collector efficiency was within 2 percent of the predicted value and the output power was within 4 percent of the predicted value. It was concluded that the low plate efficiency in this experiment was due to poor beam focusing. The dimensional control was improved and the front (nearest sole) beam forming electrode was modified.

The 13th pump down consisted of an experiment to evaluate efficiency enhancement by potential limiting. The data from this experiment are presented in the appropriate section.

The 14th pump down verified all aspects of the amplifier design and the results of this experiment follow.

7.1 Ten Stage Depressed Collector

In general the ten stage depressed collector described previously demonstrates excellent agreement with predictions. When the experimental amplifier is operating without rf output power

(zero drive) the collector efficiency can be measured directly. For a predicted 89.1 percent collector efficiency, the experimental device demonstrates 87.2 percent.

The experimental collector enhances the IBCFA efficiency over the entire rf dynamic range of the device (Figure 11) due to the uniform element spacing. In Figure 11 the amplifier is being operated at reduced output power (reduced i_b) and the basic interaction efficiency of 36 percent is increased to 58.7 percent at saturation. Below saturation this collector increases efficiency by a factor of 2 to 3. Figure 11 also demonstrates almost constant collector efficiency over the rf dynamic range of the device.

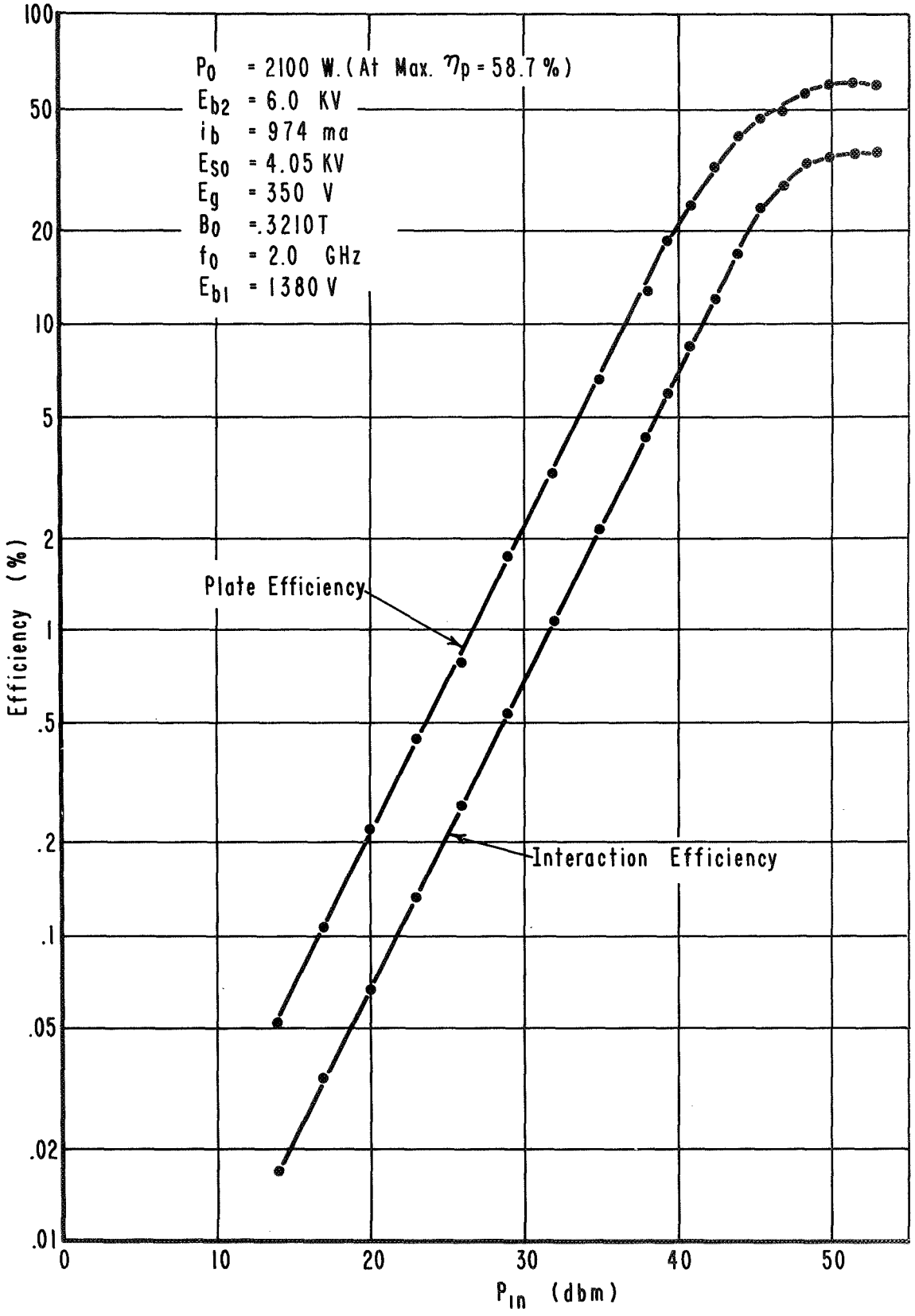

Exp. No. 2A016114 - Collector Performance D282

Fig. 11

At saturation or 15 db below saturation, the number of collector elements could be reduced to three without much sacrifice in efficiency (59.8 vs. 62.6 percent in one case). However, this three stage collector would not demonstrate the significant efficiency enhancement over a large dynamic range. The above fact is accounted for by the confinement of the beam to a small potential distribution under the above two conditions. With a small distribution of beam potential a large number of collectors is not necessary to achieve efficient collection.

This ten stage depressed collector also has another important aspect. This collector can measure the potential profile of a crossed-field beam which can be directly correlated with computer predictions of electron trajectories. If the potential, E_{cn}, of an element in the collector is changed by ΔE_{cn}, a small amount, and the current on that element changes by Δi_{cn}, then the ratio of $\Delta i_{cn}/\Delta E_{cn}$ as a function of E_{cn} represents the relative beam current as a function of beam potential (beam potential profile).

In the ideal crossed-field ribbon beam, the electrons all move parallel to the sole and circuit (laminar flow). It can be shown that for this type of beam the ratio of $\Delta i_{cn}/\Delta E_{cn}$ is constant (Appendix C).

$$\Delta i_{cn}/\Delta E_{cn} = H\epsilon_o \eta B_o \qquad (7\text{-}1)$$

In practice, the ideal electron flow is not obtained. In fact,

electron trajectories for guns similar to that used in this amplifier indicate that the best that can be expected is a beam that is 2 to 3 times thicker in potential than a laminar beam given by equation (7-1) with $\Delta i_{cn} = i_b$.

Figure 12 is a beam potential profile that is from the last experiment performed. The laminar thickness is shown on this figure. While exact correlation with computer results was not made, this profile compares favorably with some of the best computer predictions for similar gun designs. The beam in Figure 12 is not centered at zero potential because the collector is not 100 percent efficient. The movement of the beam center by collector inefficiencies should not alter the profile.

As far as can be determined, this collector offers the only direct or reliable method of experimentally evaluating a crossed-field beam. This collector should prove to be a powerful tool for crossed-field beam analysis.

7.2 Experimental Amplifier

The results from the experimental amplifier are quite encouraging (Figure 13). As expected, the 3 db saturated bandwidth of 30 MHz at 2 GHz is easily obtained. Figure 13 shows a 1 db saturated bandwidth of nearly 150 MHz at 2 GHz. Figure 13 does not show the full 3 db bandwidth due to instabilities related to the poor match obtained with the demountable system. The 3 db saturated bandwidth

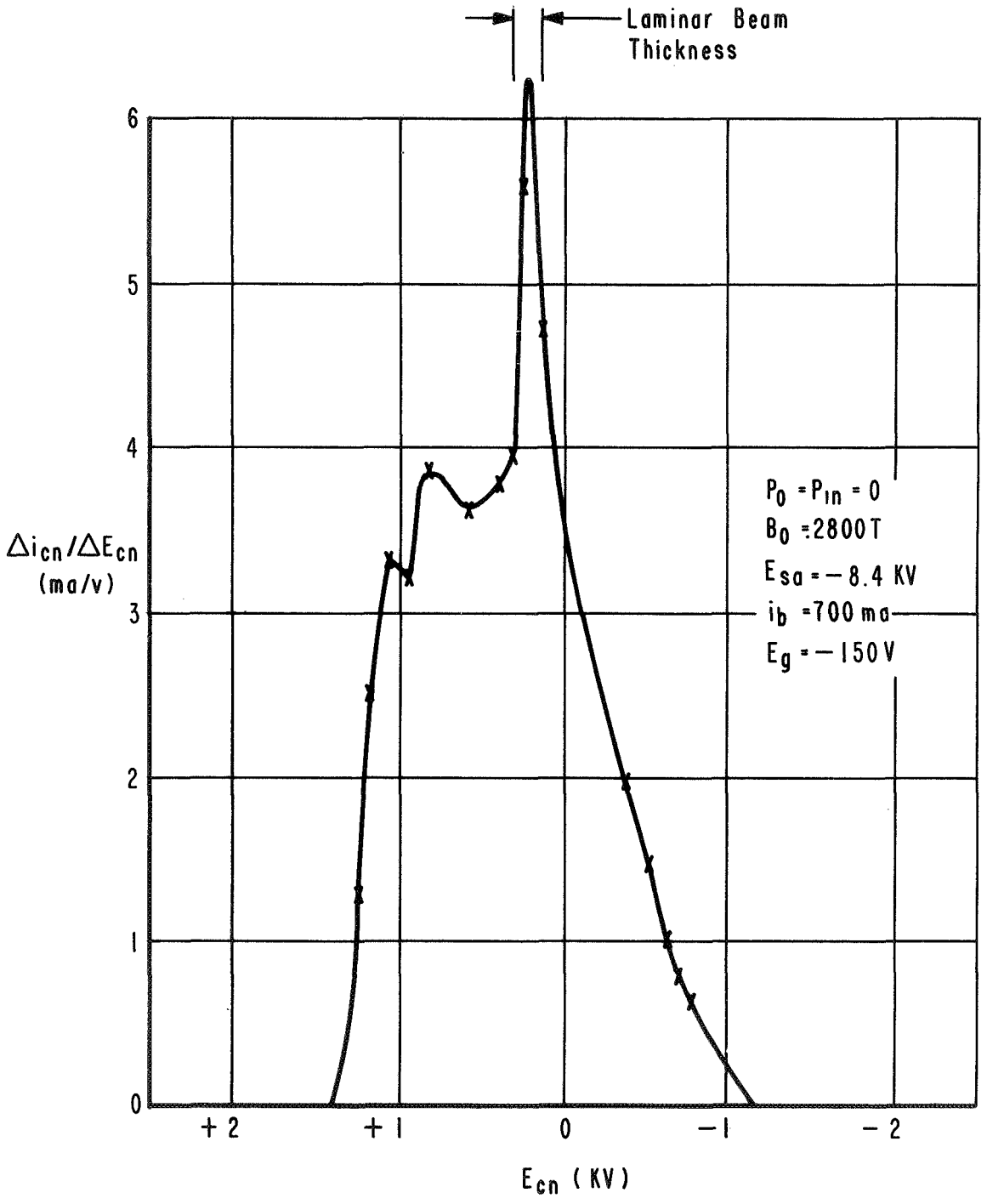

Exp. No. 2A016114 - Beam Potential Profile D283

Fig. 12

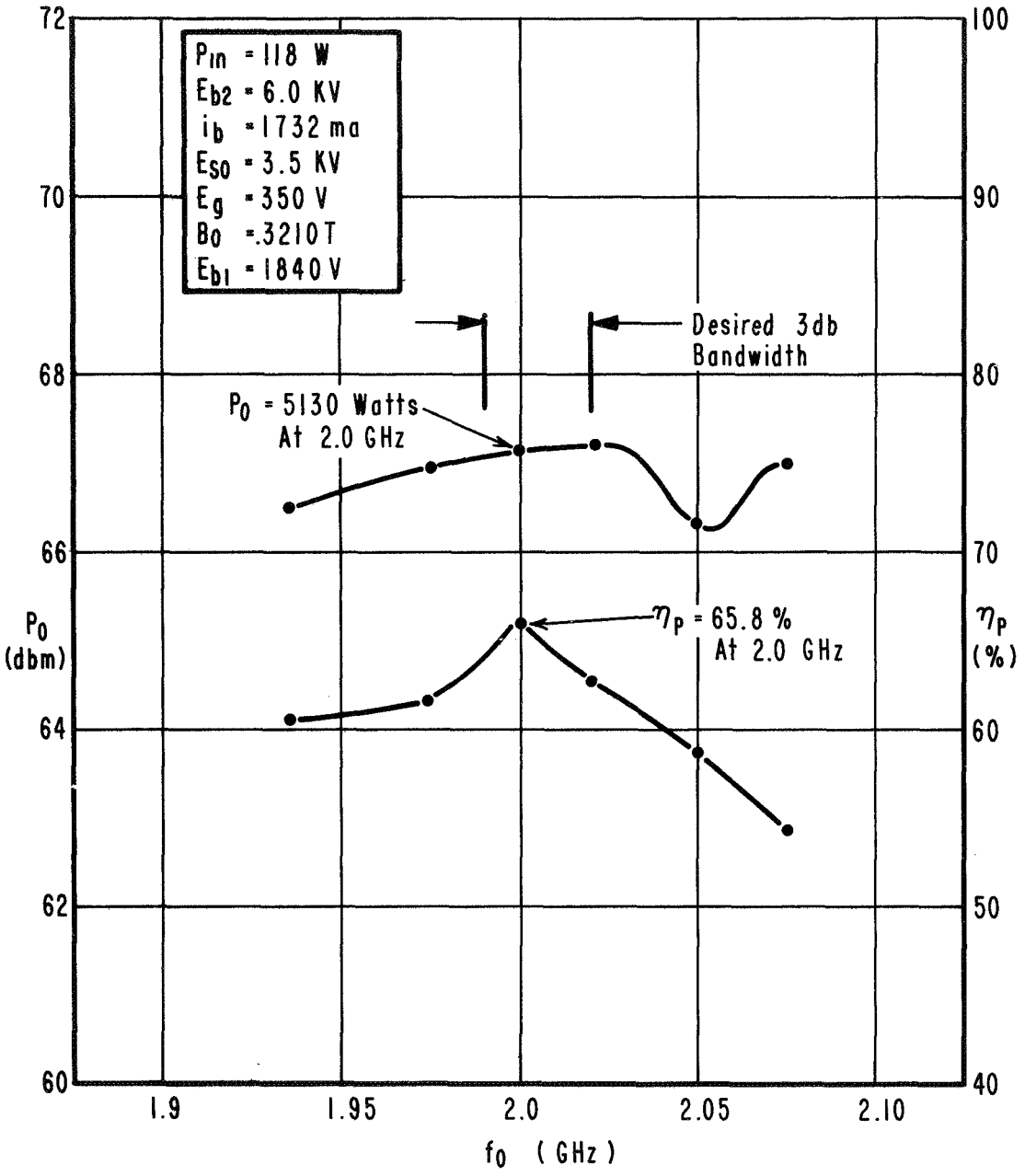

Exp. No. 2A016114 - Output Power And Plate Efficiency VS. Frequency. D284

Fig. 13

should be well in excess of 200 MHz. The desired plate efficiency of 65 percent is also demonstrated with a value of 65.8 percent.

The output match accounts for the decline of plate efficiency when moving away from 2.0 GHz. The poor output match also accounts for part of the difference between the predicted 72.9 percent plate efficiency and the measured 65.8 percent. Based on reflected power from the device, the actual plate efficiency is 69.0 percent. It is also estimated that η_p could be increased by about 3 percentage points if low drive instabilities were not present. This percentage point increase would be accomplished by increasing the beam current and decreasing the drive power, thereby lowering the level of saturation of the amplifier. The remaining discrepancy of about 1 percentage point is caused by somewhat higher circuit attenuation in the final amplifier due to brazes on the circuit. It should be pointed out that the dip in output power at 2.05 GHz in Figure 13 is also related to match.

It can be concluded from the test results that the predicted plate efficiency can be obtained in an experimental device in spite of the fact that the experimental beam is not perfect. If all electrons do not flow parallel to the sole and circuit in crossed-fields then they undergo cycloidal motion. The electrons oscillate between circuit and sole and their velocities between a maximum near the circuit and a minimum near the sole. This type of motion in the beam makes it somewhat more likely that electrons collected on the circuit

will be collected at higher velocities than predicted, thus degrading electronic efficiency. This degradation of electronic efficiency by a cycloiding beam also tends to reduce rf losses as in the calculated case. Based on the test results it appears that the degradation of electronic efficiency from a well focused but not perfect beam can be eliminated by operating at a higher electronic efficiency. The experimental device is operated at an electronic efficiency of about 92 percent as opposed to the calculated optimum value of 90 percent.

Due to the low drive instabilities caused by match, additional amplifier characteristics are presented at reduced output power (reduced i_b). Figure 14 shows the rf dynamic range of the device at midband and the 2 kw saturated output power level. The amplifier demonstrates greater than 40 db linear rf dynamic range to 3 db below saturation. The signal to noise ratio rises to 52 db at saturation and the second harmonic output power is a minimum of 34 db below the fundamental. It should be added that the background noise level is directly related to match and should be greatly improved (reduced 15 db at highest level) with an improved match.

Figure 15 shows the phase linearity, $\delta^2\phi/\delta f_o^2$ of the final experimental amplifier at the 2 kw saturated output power level. The 3 db bandwidth is about 200 MHz, well in excess of the desired 30 MHz. Over the desired bandwidth, $\delta^2\phi/\delta f_o^2$ reaches a maximum of

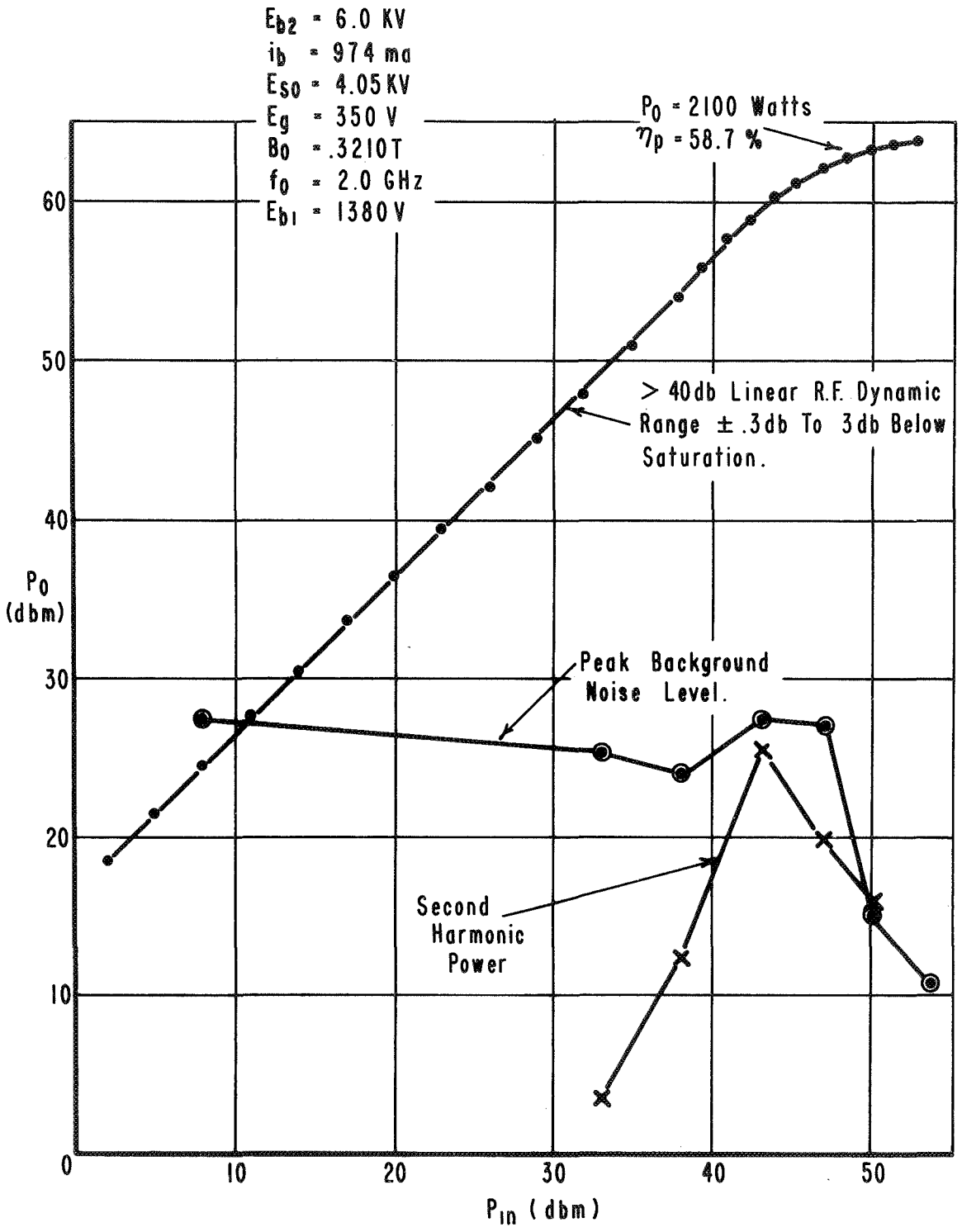

Exp. No. 2A016114 – RF Dynamic Range D285

Fig. 14

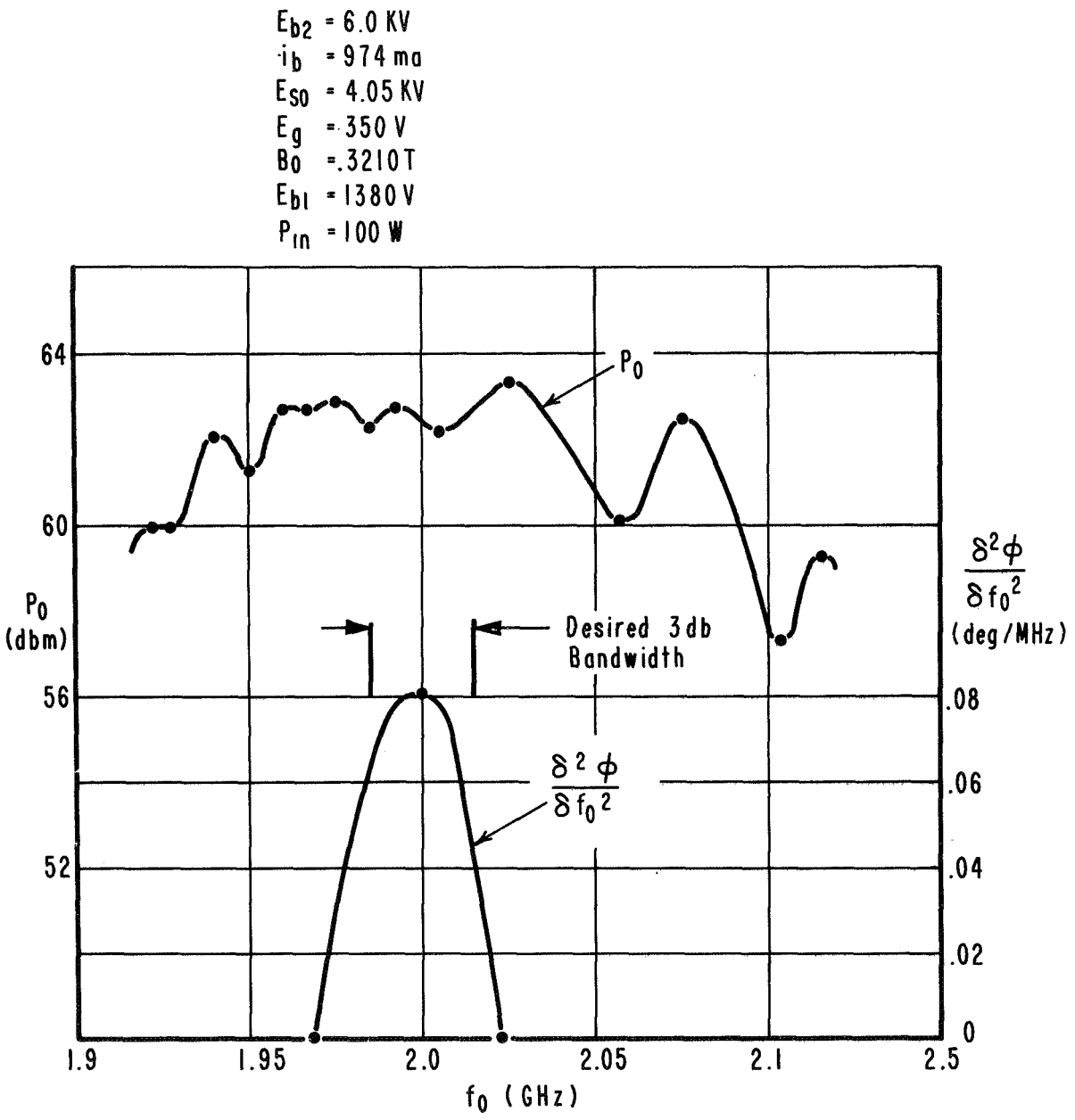

Exp. No. 2A016114 - Phase Linearity And Output Power VS. Frequency.

D286

Fig. 15

about $.08^{\circ}/MHz^{2}$. The phase non-linearity as well as the fine grain in the output power are both almost entirely due to match and not the basic crossed-field interaction.

SECTION 8

EVALUATION OF EFFICIENCY ENHANCEMENT TECHNIQUES

This work evaluates certain techniques for enhancement of the efficiency of a normal IBCFA which are not as conventional as the addition of a depressed collector. The first of these techniques is phase focusing. The work preceeding this[1] gives a more qualitative discussion of phase focusing. The specific type of phase focusing which is evaluated here is an attempt to compensate for changes in circuit velocity due to beam influence on the rf wave propagation.

The second technique for efficiency enhancement which is evaluated is beam prebunching. Beam prebunching is the formation of longitudinal bunches within the beam before the beam is injected into the main amplification region. This process normally takes place in the initial small signal region of the delay line, but it takes place rather slowly and does not form ideal bunches. Ideally the bunches would place all electrons in favorable phase. Electrons injected in unfavorable phase with the rf wave experience forces which cause them to absorb rf power. The interaction for a prebunched beam would be more rapid and therefore would have fewer rf losses and be more efficient. Several methods of prebunching a crossed field beam are evaluated.

The third efficiency enhancement technique is potential limiting. Potential limiting limits the amount of power which an unfavorably phased electron can absorb by collecting it when it reaches that potential power level. As previously discussed, the removal of the unfavorable electrons make the crossed field interaction more efficient. This technique is evaluated both analytically and experimentally.

8.1 Phase Focusing

Figure 16 shows the hot phase velocity of the final amplifier design as a function of interaction length, L. There is a maximum of 2.5 percent asynchronism resulting from the effect of the beam on circuit propagation. The maximum asynchronism only occurs over a fraction of a wave length. It is concluded that this asynchronism does not effect the interaction efficiency since it is small and is over a short electrical distance.

8.2 Beam Prebunching

Several methods for prebunching a crossed-field beam are evaluated in this section. A normal positive delay line is moved nearer to the beam for a stronger interaction in the bunching section. A negative line or line on sole, which gives power to the beam to form bunches, is evaluated as well as some combinations of these two delay lines.

Positive line beam prebunching is illustrated in Figure 17. The

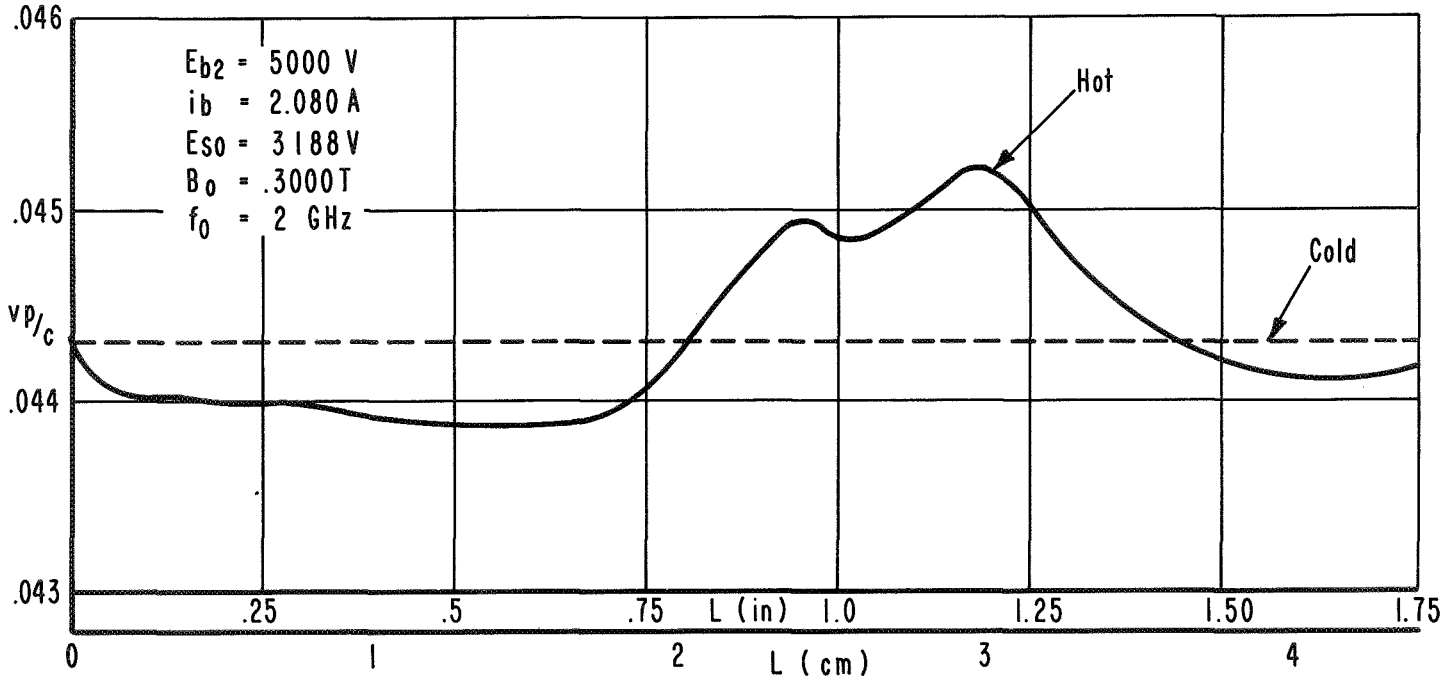

Hot Circuit Phase Velocity VS. Interaction Length D256

Fig. 16

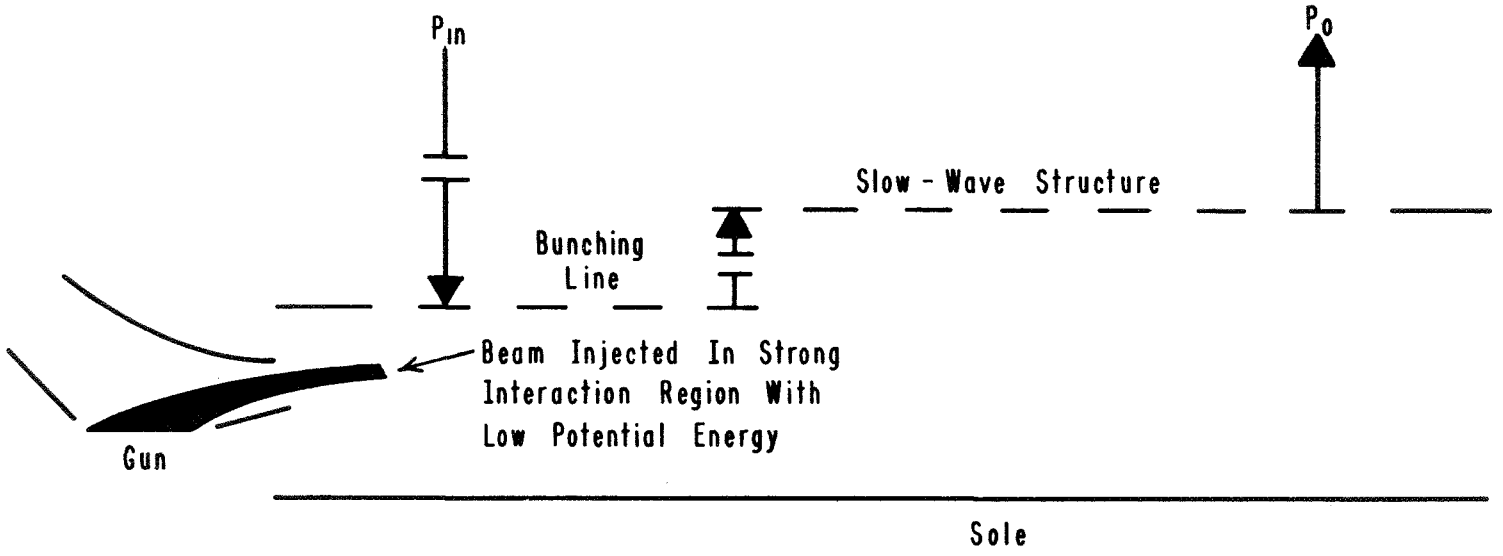

Positive Line Beam Prebunching D257

Fig. 17

bunching line has a potential between anode and cathode. The beam is injected very close to the bunching line for strong interaction with little power available. The bunches formed by this line are basically the same as those formed in the initial section of a normal interaction, i.e. favorable electrons are bunched into the most favorable phase and most unfavorable electrons remain unfavorable. While the bunches are not different from those in a normal interaction, the process takes place in a much shorter length and reduces rf losses. However, since the power level in this region is small, the losses eliminated here are not too significant. The effect of this type of prebunching is negligible in a good basic design.

Figure 18 illustrates negative line beam prebunching. The rf power on the negative line is absorbed by the beam to form bunches due to the forces exerted by the rf on the beam. These bunches are also basically the same as normal bunches, however, all of the input power is used to bunch the beam and a tighter favorably phased bunch results. This improved bunch then makes the interaction in the main amplification region more rapid and reduces rf losses.

Figure 19 represents adiabatic, no-space charge computer calculations of power vs interaction length for the final amplifier design with and without negative line beam prebunching. A faster gain rate in the high power region is obtained and the

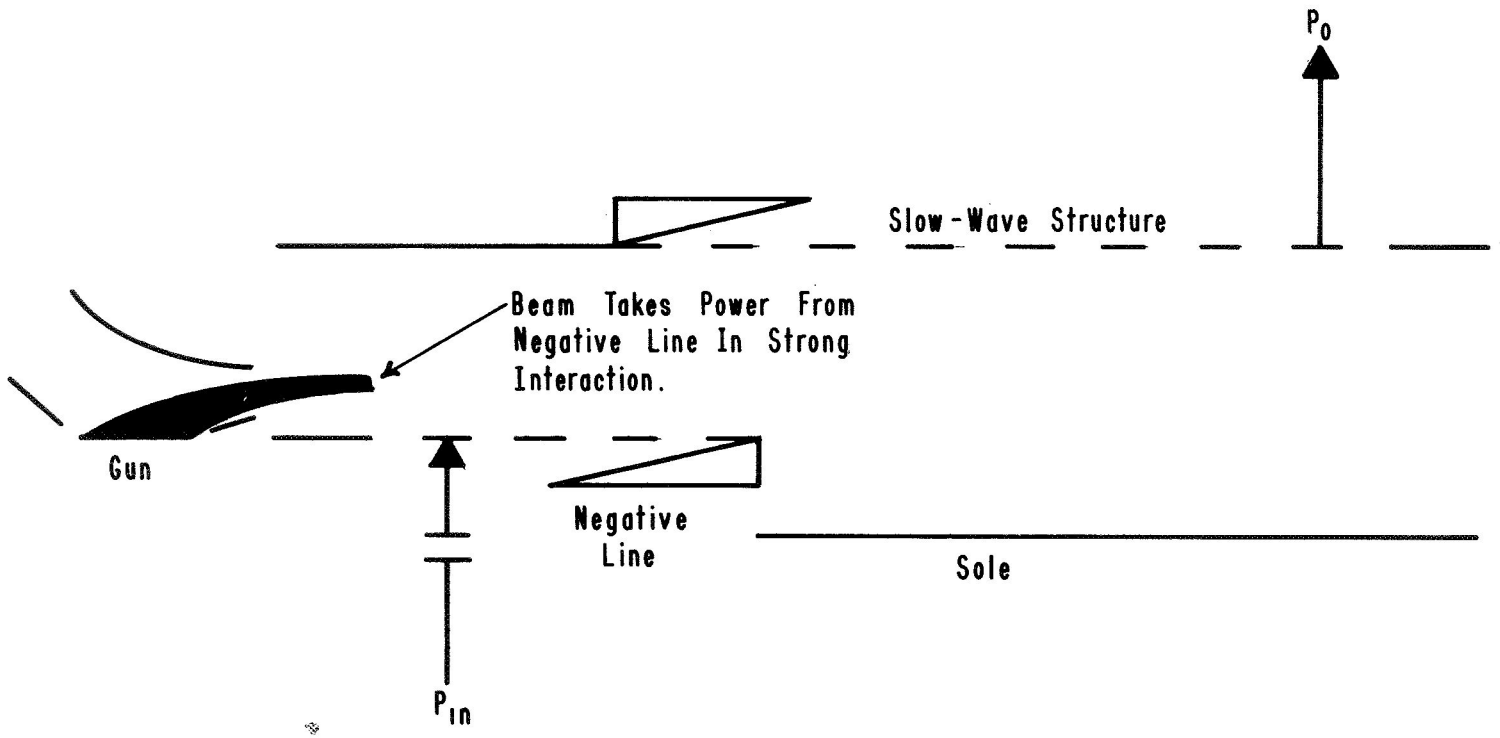

Negative Line Beam Prebunching A144

Fig. 18

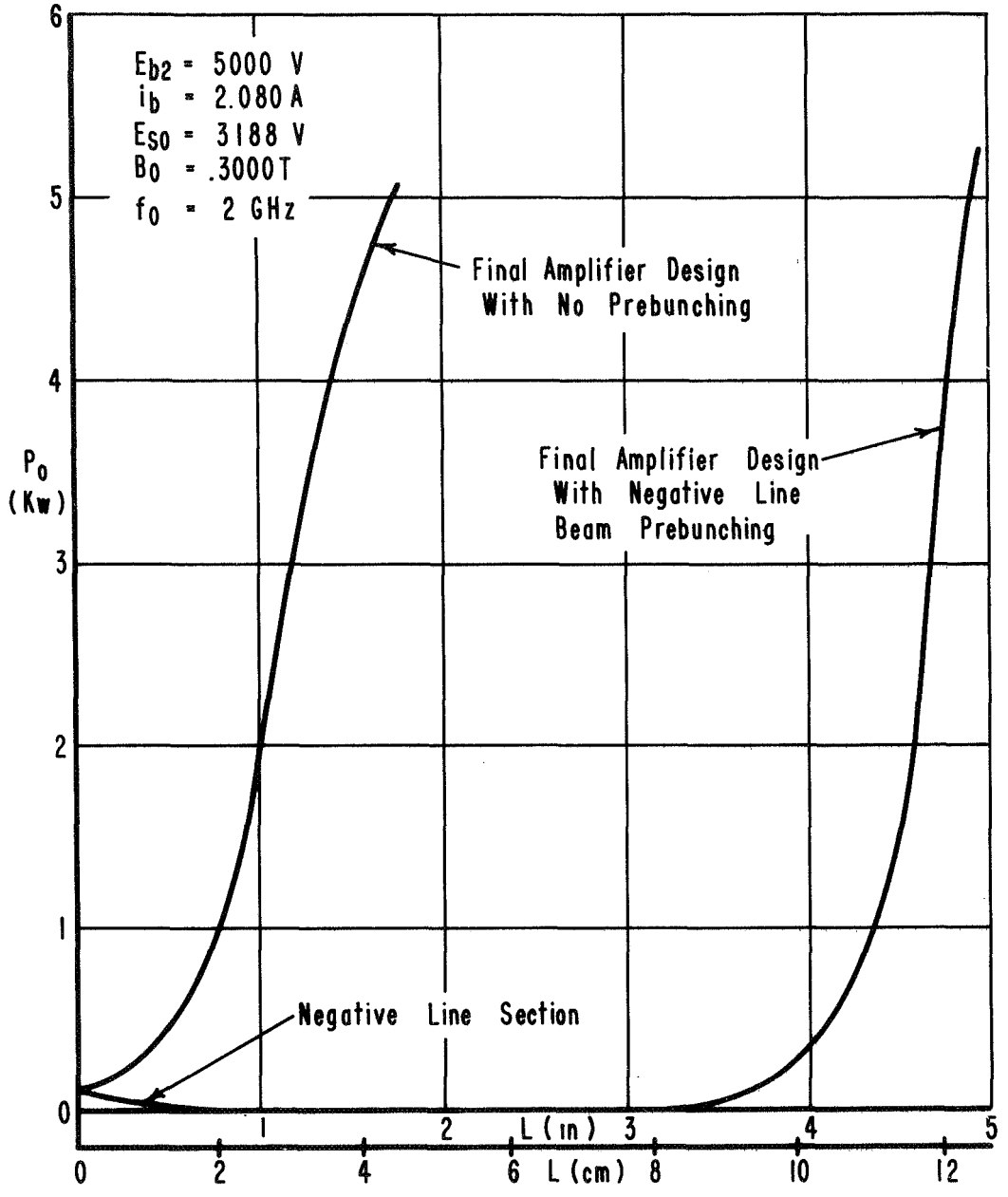

Negative Line Beam Prebunching Output Power VS. Interaction Length. D258

Fig. 19

rf losses are reduced.

It is estimated that a 2-3 percentage point increase in a plate efficiency of 72.9 percent results from the negative line prebunching. However, the length of the output section is double that of the entire normal line length. The small signal gain is then increased. Since the maintenance of low small signal gain was one of the basic assumptions in the optimization of the final amplifier design, it is believed that the 2-3 point efficiency enhancement could be obtained in the normal design if the small signal gain were allowed to increase proportionately. The negative line does not offer any real efficiency enhancement possibility unless the main delay line has a properly phased input power to reduce the gain required of it, and the results are not expected to be significant.

Figure 20 illustrates the use of both positive and negative lines driven 180 degrees out of phase. The forces on the beam are shown in a one wave length frame moving at synchronous velocity. The forces on the beam are directed to only bunch the beam and not to cause any change in beam potential. All of the power taken from the rf is used to overcome space charge forces.

The rf power required on this type of prebunching line to maintain a bunch of a given size about the most favorable phase is shown in Figure 21. The power is calculated using a charged rod (in the direction of B_o) model of the beam and the thickness is constant. The absolute power of course depends on the beam and circuits used, and Figure 21 shows only the dependence on bunch size. For the

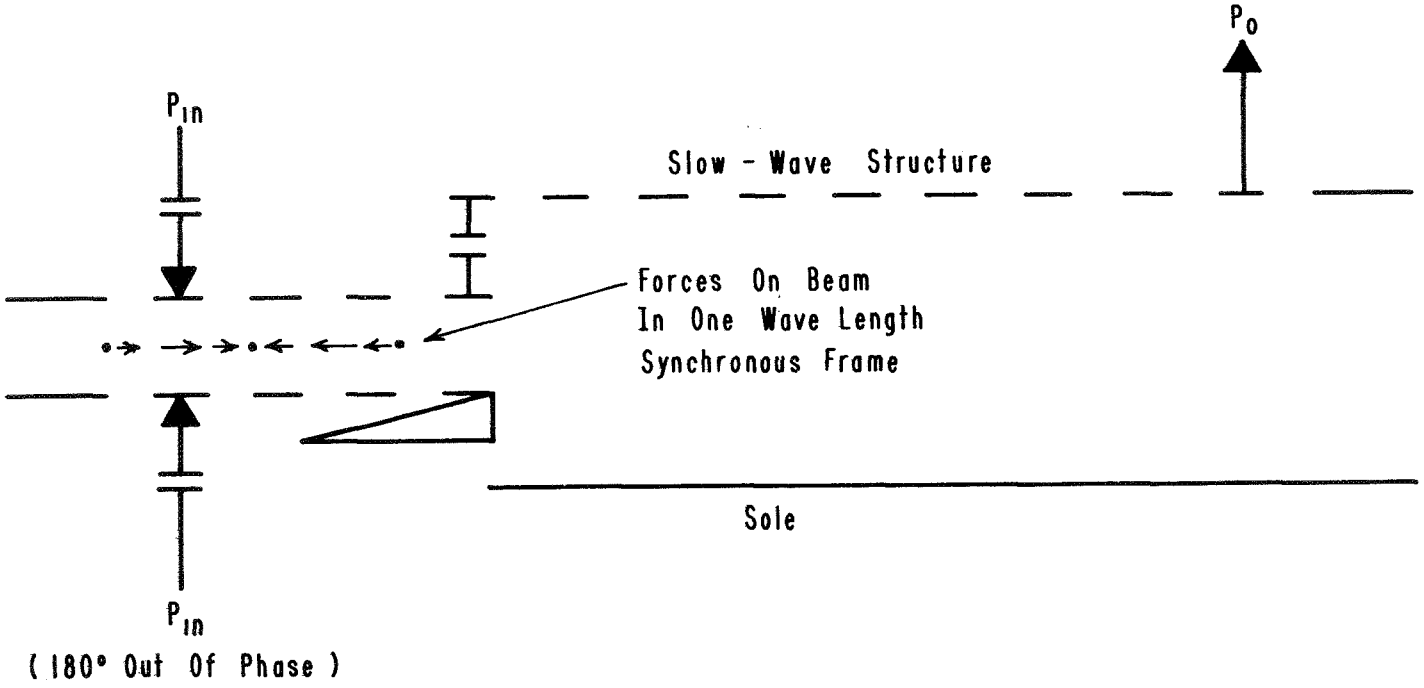

Beam Prebunching D259

Fig. 20

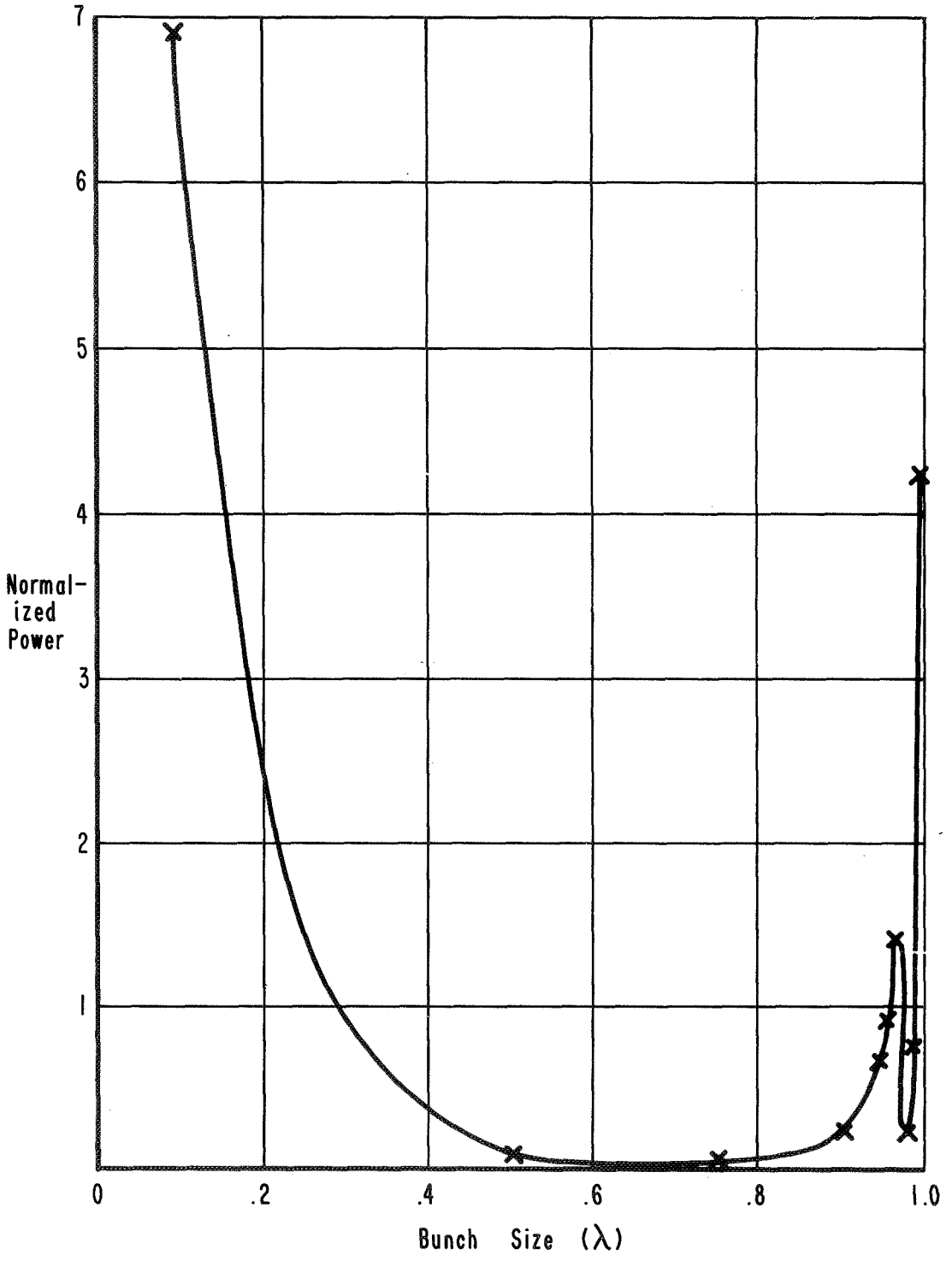

Normalized Confining Power VS. Bunch Size D260

Fig. 21

beam and circuit type of the final amplifier design the minimum power level for a single bunch is of the order of 1 kw which is much too high to be useful. The increase in required power at the one wave length bunch size indicates that unfavorable electrons will be left in that condition initially, and favorable and unfavorable bunches will be formed at more reasonable power levels much the same as a normal interaction. Significant efficiency increases are not expected from this type of prebunching.

Figure 22 illustrates the final method of beam prebunching. The bunching section is a positive line opposed to a negative line being driven in phase. Again the forces on the beam are shown in a one-wave length synchronously moving frame. Half of the beam increases in potential and half decreases resulting in no net power exchange. Hopefully most of the unfavorably phased electrons are collected on the negative line and the remaining half-wave length, favorably phased bunch is injected into the main interaction region. This method offers the possibility of increasing the gain rate in the main interaction region by many times and reducing the rf losses quite substantially. Further calculations are needed to determine to what extent the ideal half-wave length bunch can be formed and if the losses in the negative line attenuator can be made insignificant.

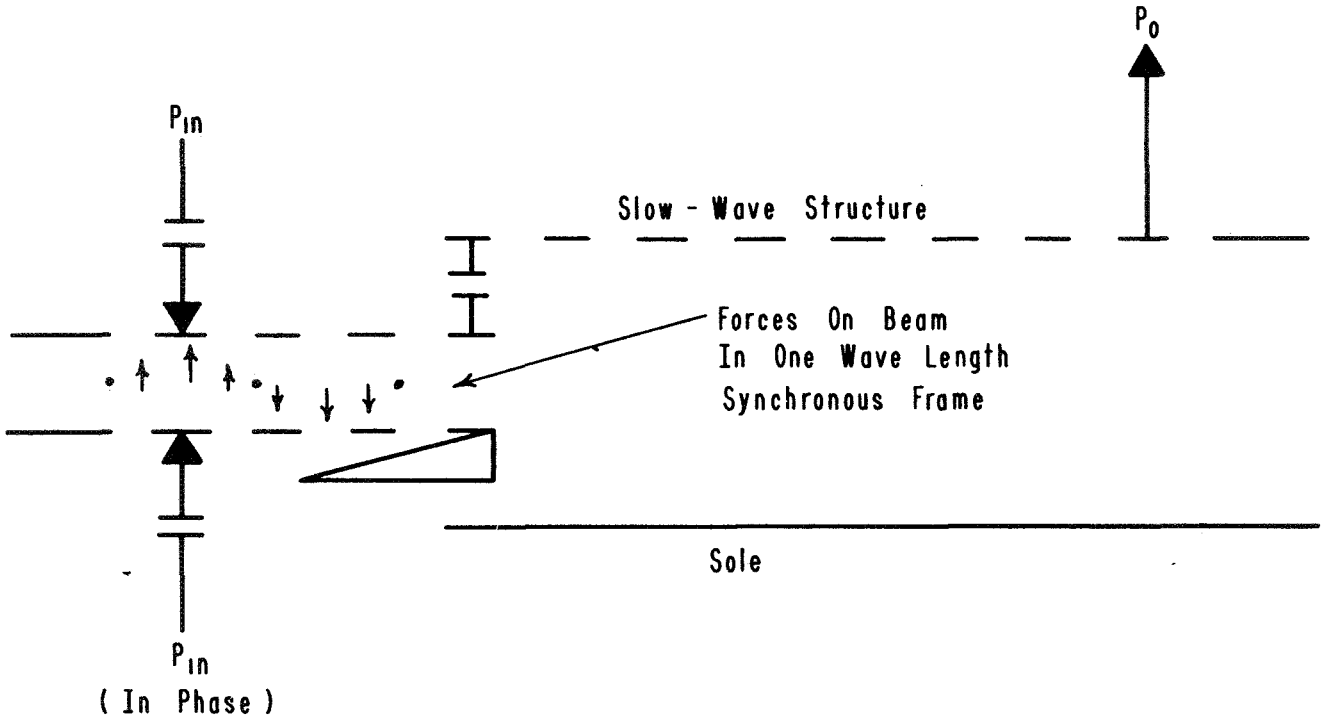

Beam Prebunching By Potenial Limiting D261

Fig. 22

8.3 Potential Limiting

Figure 23 illustrates potential limiting. The potential limiting electrodes act as distributed depressed collectors. The collection efficiency of these electrodes thus becomes quite important since the technique is used to enhance the efficiency of a device which already has an efficient depressed collector. The potential limiting electrodes (distributed depressed collector) confine the favorably phased electrons to the interaction space and exert forces to collect the unfavorably phased electrons when they reach a prescribed potential level, and hence increase interaction efficiency.

This technique for efficiency enhancement was evaluated experimentally and the results compared to predictions made for a collector efficiency equal to η_e (Figure 24). There is a good agreement between predicted increases in output power for the current collected by the potential limiting electrodes. Twenty-five percent of the beam collected on the potential limiting electrode gives a measured and predicted 4 percent increase in output power. However, the power output does not continue to increase for potential limiting voltages more positive than cathode, as predicted. This fact is due to the collection of favorable electrons at cathode potential in the real beam where the analytical model confines favorable electrons to be more positive than V_o and therefore does not allow collection at cathode potential.

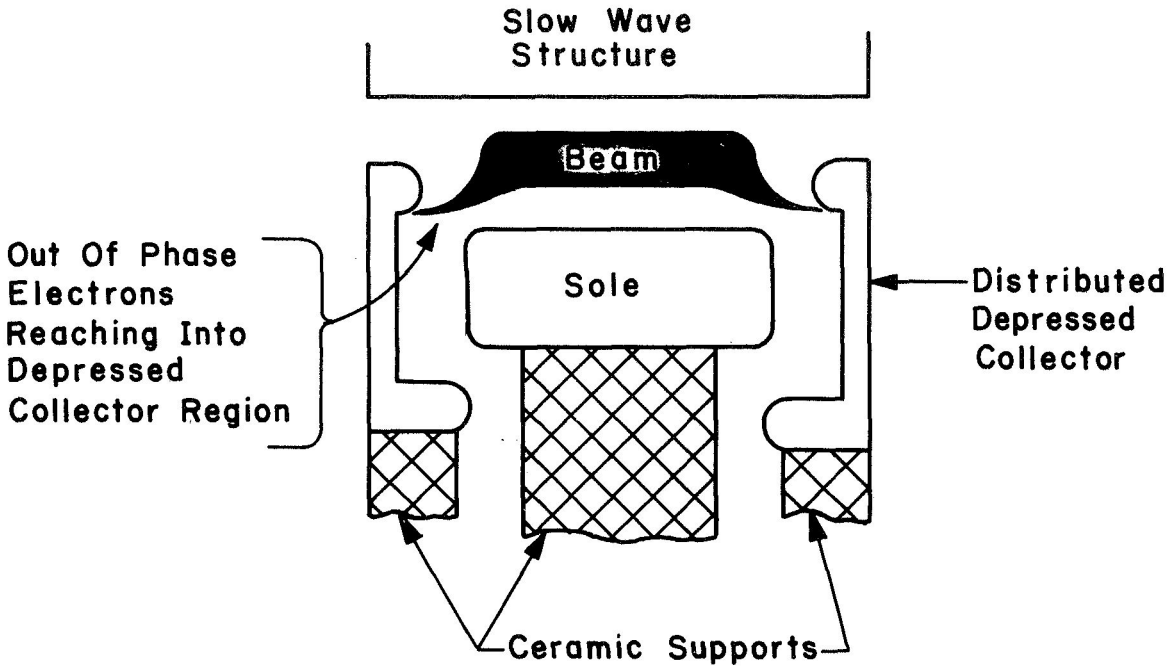

Cross-Section Of A Distributed Depressed Collector. (Potential Limiting Electrodes) A143

Fig. 23

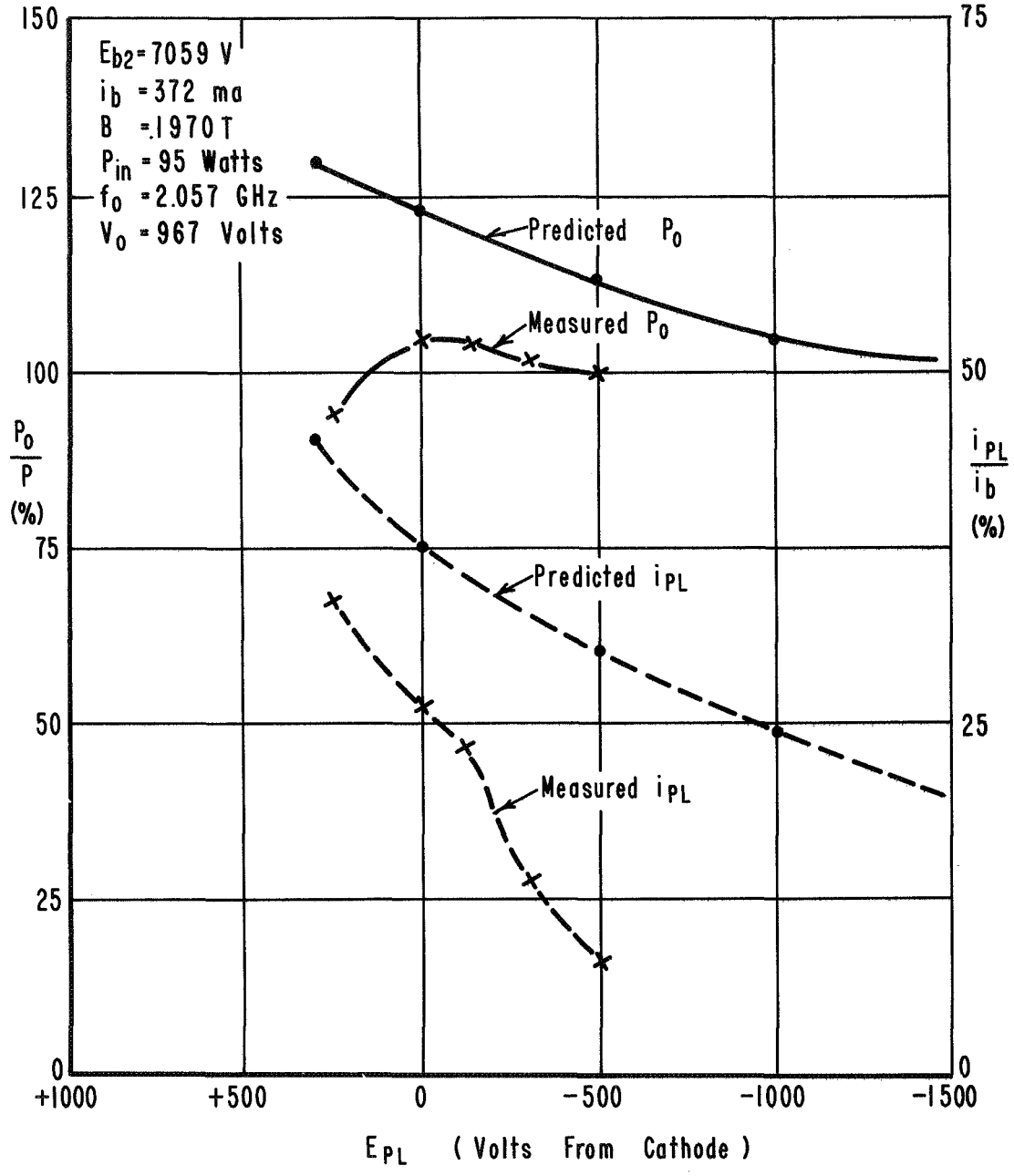

Normalized Output Power And Potential Limiting Current VS. Potential Limiting Voltage. D263

Fig. 24

The difference between the limiting potential predicted and measured for a given potential limiting current represents the power loss added to the $V_o i_{pL}$ loss. This added dissipation causes the actual collector efficiency of these electrodes to be reduced from the η_e value. This collector efficiency increases with the limiting potential (Fig. 25). In this case, at cathode potential (where interaction efficiency increase is maximum) the collector efficiency is 80 percent.

In the above case the rf losses are reduced and the collector losses increased resulting in almost no change in plate efficiency. Further study is needed to determine if operation at higher gain rates or operation where space charge is more influential will change the above result. The most appropriate use of this technique would seem to be on a device without a depressed collector or as a technique for eliminating the collector elements between cathode and sole in the present device. Potential limiting at cathode experimentally increases the efficiency by 48 percent over the device without any collector.

The efficiency enhancement techniques discussed here offer the possibility of operating at about the same efficiency but with a lower value of the space charge parameter. A lower value of S tends to decrease stability problems and linearize gain. These techniques should be studied in this regard rather than as efficiency enhancement techniques.

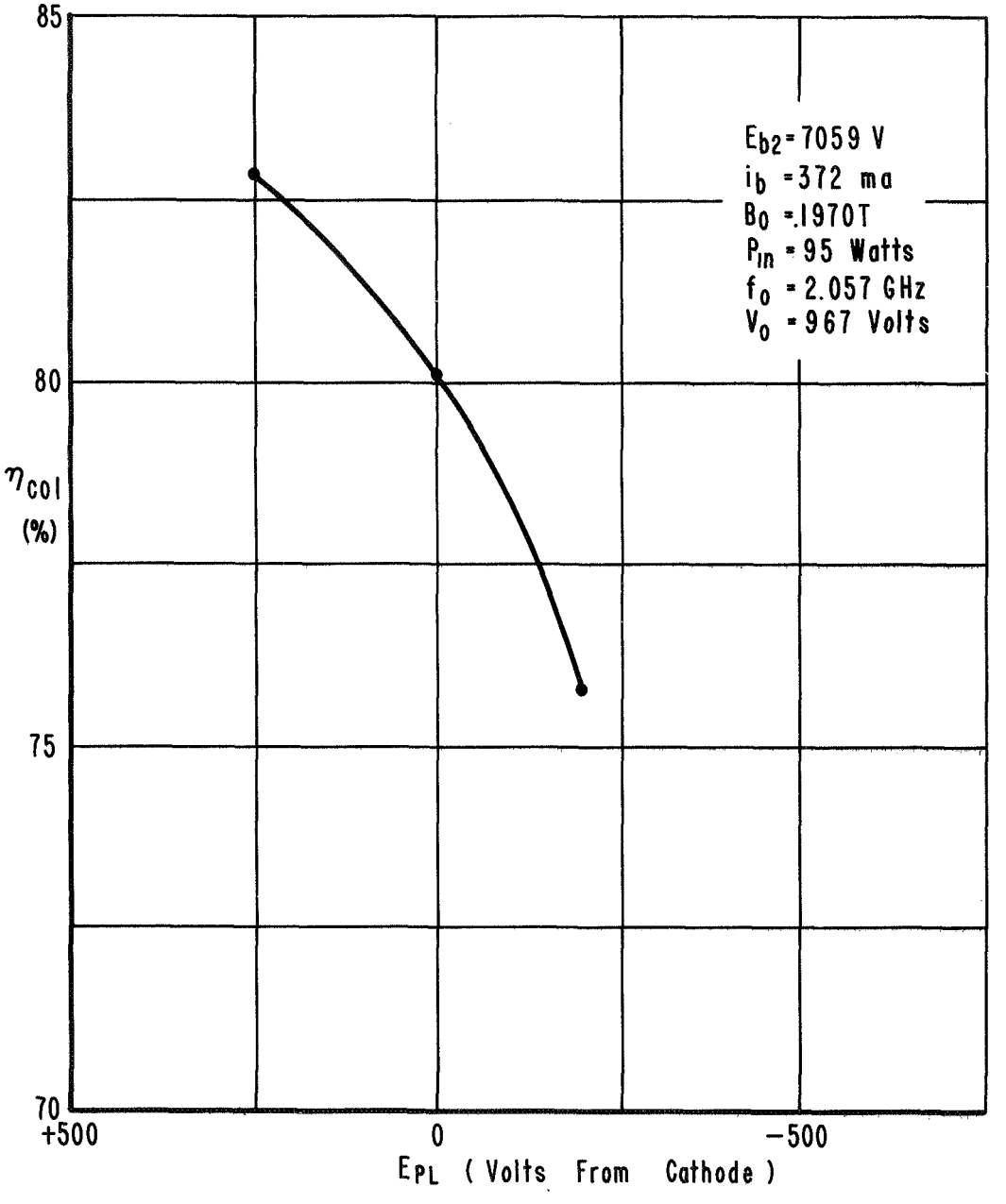

Collection Efficiency VS. Potential Limiting Electrode Voltage

D264

Fig. 25

SECTION 9

SUMMARY OF RESULTS

This report examines the design of an injected beam crossed-field amplifier (IBCFA) including a ten stage depressed collector suitable for spaceborne communications applications. The emphasis is on low cathode loading for long life (greater than 2 years), the capability of 5 kw cw output power with conduction cooling at 2 GHz with a 3 db bandwidth of at least 30 MHz, 16 db gain, and the highest possible efficiency. Since highest possible efficiency is desired, techniques other than the ten stage depressed collector are also evaluated with respect to their application to efficiency enhancement.

A very wide slow-wave circuit (approximately one-half wave length) is used in the amplifier design. The exceptional width of this circuit provides the necessary thermal dissipation capability and maintains low cathode loading. The design procedure described indicates that the circuit used has low rf losses for highly efficient operation.

The ten stage collector is predicted to make available more than 90 percent of the kinetic power in the spent beam available for collection on depressed electrodes. The collector is also predicted to recover 90 percent of the potential power in the spent

beam. In the low duty demountable experimental amplifier, the collector performance is verified with an overall collector efficiency of 87.2 percent for a predicted 89.1 percent.

The amplifier design including the ten stage collector is also verified in the low duty demountable amplifier. The plate efficiency, i.e. overall efficiency, was measured at 65.8 percent as compared to a predicted 72.9 percent. The discrepancy is accounted for by poor match and increased attenuation due to brazes which can be eliminated. The 3 db bandwidth is demonstrated to be at least 5 times greater than the desired 30 MHz at 2 GHz.

At reduced output power and gain (reduced beam current) the experimental amplifier demonstrates greater than 40 db linear rf dynamic range to 3 db below saturation with a signal to noise ratio rising to 52 db and the second harmonic power output a minimum of 34 db down from the fundamental. The phase linearity is measured to be $0.08°/MHz^2$ maximum over the 30 MHz desired bandwidth at a power level of 2 kW. The phase linearity is primarily affected by the circuit match.

Phase focusing by changing the circuit velocity to reduce asynchronism caused by beam effects on the circuit propagation is found to be a negligible value. Beam prebunching leads to minor improvements, but needs further study for complete evaluation.

Potential limiting is found to be of great value for eliminating collector elements between sole and cathode potential and for

increasing the efficiency of amplifiers without efficient collectors. Potential limiting does not affect the efficiency of the amplifier design including a ten stage collector as presented. The collector efficiency of a set of potential limiting electrodes in the experimental amplifier is greater than 80 percent at cathode potential which is the optimum operating point. The output power of the experimental amplifier is increased 4 percent by these potential limiting electrodes. The potential limiting electrodes result in a 48 percent increase in amplifier efficiency over the amplifier without any collector.

SECTION 10

DEVICE IMPROVEMENT

All of the efficiency enhancement techniques examined in this work result in small improvement (≈ 2 percentage points) at best except beam prebunching similar to potential limiting. However, this latter technique needs additional analysis before its full potential can be estimated.

The basic reason that most efficiency enhancement techniques lead to little improvement is that they tend to improve the weak interaction region. In this weak interaction region (first part of the circuit) the losses are not very significant and consequently cannot affect overall efficiency to any great extent.

One approach to improving this device is a study of the various efficiency enhancement techniques from the point of view of increasing the upper limit of the linear rf dynamic range of the device. As indicated in the optimization studies, increasing this useful rf dynamic range results in a sacrifice of overall efficiency, or increasing the saturated gain while maintaining a given useful rf dynamic range results in a sacrifice of overall efficiency. If an efficiency enhancement technique increases overall efficiency only slightly, but also increases the useful rf dynamic range or saturated gain, then more substantial

efficiency enhancement can be expected for the same gain and useful rf dynamic range.

It follows from the above discussion that another approach to improving the overall efficiency of the device is to give up saturated gain or useful rf dynamic range. Rough estimates indicate that about one percentage point in overall efficiency can be gained per db of reduction in saturated gain while maintaining the same useful rf dynamic range.

The best approach to improving this device is in finding a method for removing the requirement to include dielectric in the circuit. Other circuits (resonant cavity types in particular) should be examined with this dielectric requirement in mind. Other methods of heat transfer, such as heat pipes, should be examined as methods of removing the need for dielectric in the Karp circuit. This approach may lead to efficiencies as much as 10 percentage points higher. Note the severe restrictions that the use of dielectric imposed on the circuit quality factor and available circuit width in the optimization studies.

SECTION 11

SYMBOLS

a	sole to line gap
B_o	dc magnetic field
B.W.	3 db bandwidth
c	velocity of light
D	gain parameter
E	potential relative to cathode
E_1	dc electric field at collector elements
E_{b1}	peak accelerator to cathode voltage
E_{b2}	anode to cathode voltage
E_{cn}	n^{th} collector to cathode voltage
E_f	filament to cathode voltage
E_g	grid to cathode voltage
E_o	dc electric field in the interaction region
E_{max}	maximum dc electric field without arcing
E_{pL}	potential limiting electrode to cathode voltage
E_{sa}	sole to anode voltage
E_{so}	sole to cathode voltage
f_o	operating frequency
H	beam width in the direction of magnetic field
i	peak current
i_b	peak beam current
i_{b1}	peak accelerator current

i_{b2}	peak anode current
i_{cn}	n^{th} collector peak current
I_f	filament current
i_g	peak grid current
i_{pL}	peak potential limiting electrode current
i_{so}	peak sole current
J	beam current density
K	electronic efficiency degradation factor
K_o	interaction impedance
L	interaction length
N	total number of collectors
n	collector number from sole
p_{col}	peak input power to the collector region
p_{in}	peak rf input power
p_o	peak rf output power
Q	2π times the ratio of energy stored to energy dissipated per cycle
S	space charge parameter
x	position measured from the sole
x_o	beam center measured from the sole
v_e	electron average or drift velocity
v_p	circuit phase velocity
V_o	beam voltage relative to cathode
α	circuit attenuation in db per wavelength
α_T	total rf losses on the slow-wave circuit

β	circuit propagation constant
$\beta p/\pi$	phase shift per cell relative to 180^{o}
ϵ_{o}	permittivity of free space
η	electron charge to mass ratio
η_{col}	collector efficiency
η_{e}	electronic efficiency
η_{p}	plate efficiency (overall efficiency)
λ	wavelength of circuit wave
ρ	beam space charge density
ϕ	rf phase shift
ω_{c}	cyclotron frequency
ω_{p}	beam plasma frequency

SECTION 11

REFERENCES

1. Jones, C.L. and Orr, J.E.: Analytic Design of a 2.0 GHz Space Borne Linear Injected Beam Crossed Field Amplifier. NASA CR 72392, October, 1968.

2. Karp, A.: Traveling-Wave Tube Experiments at Millimeter Wavelength With a New Easily Built Space Harmonic Circuit. IRE, Vol. 43, No. 1, January, 1955, pp. 41-46.

3. Pierce, J.R.: Traveling-Wave Tubes. D. Van Nostrand, Inc., 1950, pp. 95-96.

4. Walling, J.C.: Interdigital and Other Slow Wave Structures. Journal of Electronics and Control, Vol. 3, 1957, pp. 239-258.

5. Fletcher, R.C.: A Broad-Band Interdigital Circuit for Use in Traveling-Wave Type Amplifiers. IRE, Vol. 40, No. 2, August, 1952, pp. 951-958.

6. Kino, G.S.: A New Type of Crossed-Field Electron Gun. Crossed Field Microwave Devices, Vol. 1, edited E. Okress, Academic Press, 1961, pp. 164-177.

7. Pease, M.C.: Beam Launching in High Power Crossed-Field Tubes. Crossed Field Microwave Devices, Vol. 1, edited E. Okress, Academic Press, 1961, pp. 142-143.

APPENDIX A

OPTIMUM RELATIVE BEAM INJECTION POSITION

From the condition of synchronism, we can write the product βa in terms of the frequency, the dc magnetic field, the beam voltage and the sole to line voltage.

$$\beta a = 2\pi f_o \, (-E_{sa})/(2\eta B_o V_o) \tag{A-1}$$

η is the electron charge to mass ratio.

The relative beam injection position, x_o/a, can be written in terms of the anode voltage, the sole to line voltage and the beam voltage.

$$x_o/a = 1 - (E_{b2} - V_o)/(-E_{sa}) \tag{A-2}$$

Using the definition of $\eta_e = 1 - V_o/E_{b2}$, the quantities βa and $2\beta x_o$ can now be written in terms of x_o/a.

$$\beta a = 2\pi f_o \left(\frac{\eta_e}{1-\eta_e}\right) \Big/ \left[2\eta B_o \, (1 - x_o/a)\right] \tag{A-3}$$

$$2\beta x_o = 2\pi f_o \left(\frac{\eta_e}{1-\eta_e}\right) \Big/ \left[\eta B_o \, (-1 + a/x_o)\right] \tag{A-4}$$

The term we seek to maximize can be written in terms of x_o/a.

$$\frac{\sinh 2\beta x_o}{\sinh^2 \beta a} = \frac{\sinh\left[\dfrac{2\pi f_o\left(\dfrac{\eta_e}{1-\eta_e}\right)}{\eta B_o(-1+a/x_o)}\right]}{\sinh^2\left[\dfrac{2\pi f_o\left(\dfrac{\eta_e}{1-\eta_e}\right)}{2\eta B_o(1-x_o/a)}\right]} \tag{A-5}$$

Differentiating the above equation with respect to x_o/a and setting the result equal to zero leads to the following relation.

$$\frac{1}{(1-x_o/a)^2} \tanh\left[\frac{2\pi f_o\left(\frac{\eta_e}{1-\eta_e}\right)}{\eta B_o\left(\frac{a}{x_o}-1\right)}\right] =$$

$$\frac{1}{(x_o/a)^2} \tanh\left[\frac{2\pi f_o\left(\frac{\eta_e}{1-\eta_e}\right)}{2\eta B_o\ (1-x_o/a)}\right] \qquad \text{(A-6)}$$

Using the fact that the argument of the tanh function is small and $\tanh\theta = \theta$ for small θ, a simple cubic equation is obtained.

$$2(x_o/a)^3 - (x_o/a)^2 + 2(x_o/a) - 1 = 0 \qquad \text{(A-7)}$$

Factoring the above equation we find only one real root, $x_o/a = .5$. This leads to the following maximum value for the term in question at $x_o/a = .5$

$$\left(\frac{\sinh 2\beta x_o}{\sinh^2 \beta_a}\right)_{max} = \frac{1}{\sinh\left[\frac{2\pi f_o\left(\frac{\eta_e}{1-\eta_e}\right)}{\eta B}\right]} \qquad \text{(A-8)}$$

APPENDIX B

OPTIMUM BEAM VOLTAGE

Assuming $x_o/a = .5$ and $\beta = E_{max}\sqrt{2\eta V_o}$ and all other parameters of equation (4-6) are fixed, the right hand side of equation (4-6) can be written in terms of V_o.

$$\alpha_T/p_o \sim \frac{\sinh\left[\frac{2\pi f_o\sqrt{2\eta V_o}\left(\frac{\eta_e}{1-\eta_e}\right)}{\eta E_{max}}\right]}{\sqrt{V_o}} \tag{B-1}$$

Differentiating and setting the result equal to zero leads to the following relation for the optimum V_o for minimum α/p_o.

$$\tanh\left[\frac{2\pi f_o\sqrt{2\eta V_o}\,\frac{\eta_e}{1-\eta_e}}{\eta E_{max}}\right] = \frac{2\pi f_o\sqrt{2\eta V_o}\left(\frac{\eta_e}{1-\eta_e}\right)}{\eta E_{max}} \tag{B-2}$$

The solution to the above equation is for the argument of tanh = 0. However, the equation is valid within 1 percent for the argument less than or equal to 0.2. This approximation leads to the following solution for the optimum V_o.

$$\sqrt{2\eta V_o} \leq \frac{0.2\ \eta E_{max}\eta_e}{2\pi f_o(1-\eta_e)} \tag{B-3}$$

APPENDIX C

LAMINAR BEAM POTENTIAL PROFILE

It is well known that the condition for parallel electron flow (laminar flow) in crossed fields is that $\omega_p = \omega_c$ where ω_p is the plasma frequency and ω_c is the cyclotron frequency. From the definition of the above quantities, $\omega_p = \omega_c$ implies that the beam space charge density can be written in terms of β_o and η.

$$\rho = \epsilon_o \eta B_o^2 \tag{C-1}$$

The current Δi in the region x_1 to x_2 where x is measured from the sole can be written in terms of the beam width H and the beam current density J.

$$\Delta i = H \int_{x_1}^{x_2} J dx \tag{C-2}$$

Expressing J in terms of potential E relative to cathode and space charge density ρ, equation (C-2) can be rewritten.

$$\Delta i = H\rho \int_{E(x_1)}^{E(x_2} \sqrt{2\eta E} \; \frac{dx}{dE} \; dE \tag{C-3}$$

For a laminar dx/dE can be found.

$$dx/dE = 1/\sqrt{2\eta B_o^2 E} \tag{C-4}$$

Using equations (C-1) and (C-4), equation (C-3) now reduces to a simple form.

$$\Delta i = H\epsilon_o \eta B_o \int_{E(x_1)}^{E(x_2)} dE \qquad (C\text{-}5)$$

Equation (C-5) gives the desired result for a laminar beam.

$$\Delta i/\Delta E = H\epsilon_o \eta B_o \qquad (C\text{-}6)$$

DISTRIBUTION LIST

FOR

FINAL REPORT

CR 72810

		Copies
National Aeronautics & Space Administration Headquarters Washington, D. C. 20546		
Attention:	SA/L. Jaffe	1
	SCC/A.M.C. Andrus	10
	SC/R. B. Marsten	1
NASA-Lewis Research Center 21000 Brookpark Road Cleveland, Ohio 44135		
Attention:	C. C. Conger (M.S. 54-1)	1
	R. E. Alexovich (M.S. 54-5)	1
	Dr. H. G. Kosmahl (M.S. 54-5)	1
	Technology Utilization Officer (M.S. 3-19)	1
	Library (M.S. 60-3)	2
	Report Control Office (M.S. 5-5)	1
	N. T. Musial (M.S. 500-311)	1
	G. J. Chomos (M.S. 54-5)	50
	Rockets and Spacecraft Procurement Section (M.S. 500-313)	1
Communication Systems, Inc. 5817 Columbia Pike Falls Church, Virginia 22046		
Attention:	J. Bisaga	1
Rand Corporation 1700 Main Street Santa Monica, California 90404		
Attention:	Dr. J. Holt	1
NASA-George C. Marshall Space Flight Center Huntsville, Alabama 35812		
Attention:	RASTR-A/E. C. Hamilton	1
	Library	1

		Copies
NASA-Goddard Space Flight Center Greenbelt, Maryland 20771		
Attention:	733/R. Pickard	1
	Library	1
NASA-Ames Research Center Moffett Field, California 94035		
Attention:	OART/MOA/E. Van Vleck (M.S. 202-6)	1
	Library	1
NASA-Langley Research Center Langley Station Hampton, Virginia 23365		
Attention:	B. Kendall (M.S. -173)	1
	Library (M.S. -185)	1
NASA-Manned Spacecraft Center Houston, Texas 77001		
Attention:	Library	1
Jet Propulsion Laboratory 4800 Oak Grove Drive Pasadena, California 91103		
Attention:	L. Derr	1
	Library	1
NASA Scientific and Technical Information Facility P.O. Box 33 College Park, Maryland 20740		
Attention:	NASA Representative	3
TRW Systems One Space Park Redondo Beach, California 90278		
Attention:	W. A. Finley/Space Vehicle Division	1
General Dynamics, Convair Division P.O. Box 1128 San Diego, California 92112		
Attention:	F. J. Dore/Advanced Programs Laboratory	1
Hughes Aircraft Company Space Systems Division 1194 W. Jefferson Boulevard Culver City, California 90230		
Attention:	H. A. Rosen/Satellite Systems Laboratory	1

	Copies
General Electric Company Missile and Space Division Valley Forge Space Technology Center P.O. Box 8555 Philadelphia, Pennsylvania 19101	
Attention: H. Collins	1
P. Nadler	1
Federal Communications Commission 521 Twelfth Street Washington, D. C. 20554	
Attention: M. Fine	1
U. S. Information Agency 25 "M" Street, S. W. Washington, D. C. 20547	
Attention: IBS/EF/G. Jacobs	1
General Electric Company Tube Department Microwave Tube Business Section Schenectady, New York 12305	
Attention: R. Dehn	1
Litton Industries Electron Tube Division 960 Industrial Road San Carlos, California 94070	
Attention: Dr. G. Pokorny	1
J. Orr	1
W. Day	1
Dr. O. Sauseng	1
SFD Laboratories, Inc. 800 Rahway Avenue Union, New Jersey 07083	
Attention: Dr. G. Farney	1
Hughes Aircraft Company Electron Dynamics Division P.O. Box 2999 Torrance, California 90509	
Attention: Dr. J. Mendel	1
Dr. T. Tammaru	1

	Copies
Watkins Johnson Company 333 Hillview Avenue Palo Alto, California 94304	
Attention: Dr. D. Watkins	1
Varian Associates 611 Hansen Way Palo Alto, California 94303	
Attention: Dr. G. Caryotakis	1
Dr. J. Rentz	1
Radio Corporation of America Industrial Tube Division Lancaster, Pennsylvania 17604	
Attention: W. P. Bennett	1
Raytheon Company Research Division 28 Seyon Street Waltham, Massachusetts 02154	
Attention: W. Teich	1
Dr. J. M. Osepchuk	1
Mr. Lawrence Gasch Aerospace Radar Branch U. S. NRL Washington, D. C. 20390	1
Mr. Robert Richardson Mail No. 1620 Martin-Marietta Corporation Denver Division P.O. Box 179 Denver, Colorado 80201	1
Mr. William E. Waters Sr. Engineer Staff Specialist 3939 Fabian Way M.S. C-70 Palo Alto, California 94303	1
Mr. George Orr Code 733 Goddard Space Flight Center Greenbelt, Maryland 20771	1

	Copies
Sperry Electronic Tube Division Gainesville, Florida 32601	
Attention: H. H. Conners	1
Naval Electronic Systems Command PME 116 Washington, D. C. 20360	
Attention: Lt. Commander L. Wardel	1